HHS Public Access

Author manuscript

Cell. Author manuscript; available in PMC 2024 August 31.

Published in final edited form as:

Cell. 2023 August 31; 186(18): 3862–3881.e28. doi:10.1016/j.cell.2023.07.021.

A neural circuit for male sexual behavior and reward

Daniel W. Bayless[1,†], **Chung-ha O. Davis**[2,†], **Renzhi Yang**[1,†], **Yichao Wei**[1], **Vinicius Miessler de Andrade Carvalho**[1], **Joseph R. Knoedler**[1], **Taehong Yang**[1], **Oscar Livingston**[1], **Akira Lomvardas**[1], **Gabriela J. Martins**[9], **Ana Mafalda Vicente**[9,10], **Jun B. Ding**[3,4], **Liqun Luo**[5,6], **Nirao M. Shah**[1,7,8,*]

[1]Department of Psychiatry and Behavioral Sciences, Stanford University, Stanford, CA 94305.

[2]Stanford Neurosciences Graduate Program, Stanford University, Stanford, CA 94305.

[3]Department of Neurosurgery, Stanford University, Stanford, CA 94305.

[4]Department of Neurology and Neurological Sciences, Stanford University, Stanford, CA 94305.

[5]Department of Biology, Stanford University, Stanford, CA 94305.

[6]Howard Hughes Medical Institute, Stanford University, Stanford, CA 94305.

[7]Department of Neurobiology, Stanford University, Stanford, CA 94305.

[8]Department of Obstetrics and Gynecology, Stanford University, Stanford, CA 94305.

[9]Allen Institute for Neural Dynamics, Seattle, WA 98109

[10]Zuckerman Mind Brain Behavior Institute, Columbia University, New York, NY 10027.

SUMMARY

Male sexual behavior is innate and rewarding. Despite its centrality to reproduction, a molecularly-specified neural circuit governing innate male sexual behavior and reward remains to be characterized. We have discovered a developmentally-wired neural circuit necessary and sufficient for male mating. This circuit connects chemosensory input to BNSTpr^{Tac1} neurons, which innervate POA^{Tacr1} neurons that project to centers regulating motor output and reward. Epistasis studies demonstrate that BNSTpr^{Tac1} neurons are upstream of POA^{Tacr1} neurons, and BNSTpr^{Tac1}-released Substance P following mate recognition potentiates activation of POA^{Tacr1}

Correspondence: nirao@stanford.edu.
†Equal contributions
*Lead contact

AUTHOR CONTRIBUTIONS

Conceptualization, DWB, COD, RY, LL, NMS; methodology, DWB, COD, YW, RY; investigation, VMAC, DWB, COD, AL, OL, YW, RY; analysis VMAC, DWB, COD, JBD, JRK, GJM, AMV, YW, RY; writing, DWB, COD, RY, NMS; review and editing, DWB, COD, JBD, RY, LL, NMS; visualization, DWB, VMAC, COD, YW, RY, NMS; supervision, DWB, COD, LL, NMS; funding, VMAC, COD, JBD, LL, YW, RY, NMS.

DECLARATION OF INTERESTS

LL is a member of the advisory board for Cell; DWB, COD, JRK, NMS are named inventors on a patent application that has been filed on the subject matter; AL is son of and NMS is a co-founder of Yemaya.

neurons through Tacr1 to initiate mating. Experimental activation of POA^{Tacr1} neurons triggers mating, including in sexually-satiated males and is rewarding such that it elicits dopamine release and self-stimulation of these cells. Together, we have uncovered a neural circuit that governs the key aspects of innate male sexual behavior: motor displays, drive, and reward.

In brief statement

Molecular genetics, neuronal activity monitoring, and circuit epistasis reveal a developmentally-wired neural circuit for male sexual behavior that senses pheromones, recognizes mates, triggers mating, and governs sexual drive and reward.

Graphical Abstract

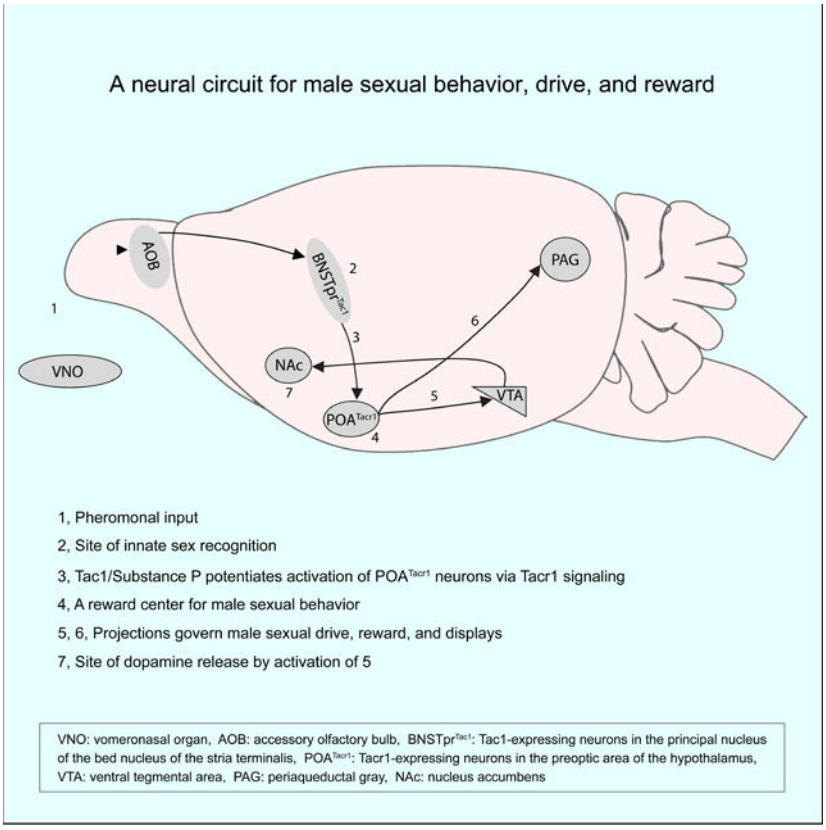

INTRODUCTION

Mating, an essential social behavior, is developmentally-wired into the brain and can be performed without prior experience. This innate program enables animals to procreate upon sexual maturation and is especially advantageous if encounters with potential mates are infrequent. Indeed, feral mice are solitary, individual males can occupy large territories[1,2], and sexually naive males mate with females[3]. Despite the experimental tractability of developmentally-patterned processes in mice, a molecularly-specified neural circuit that governs male mating remains to be defined.

Chemosensory cues are critical for detecting potential mates and eliciting sexual behavior[4–8]. Male BNSTpr^{Tac1} neurons utilize chemosensory cues to distinguish between sexes and guide mating toward females and aggression toward males[9,10]. Other neuronal populations are also critical for male mating, including most prominently the preoptic area of the hypothalamus (POA)[11–18], but these do not appear to encode sex of conspecifics in sexually naive males, their molecular identity remains to be defined, and they regulate both mating and aggression[9–12,15–27]. Indeed, it has been challenging to pinpoint neurons that regulate male mating but not aggression. These findings have led to a model in which mating, aggression, and other social behaviors are regulated by a common set of brain regions, including the principal nucleus of the bed nucleus of the stria terminalis (BNSTpr) and POA, such that these behaviors arise as an emergent output of the network[24,28–33]. Finally, most studies on mating have been done in sexually experienced males. Recent work on these neuronal populations reveals significant plasticity in response to internal states and social experience, thereby rendering it difficult to discern their contribution to innate displays of mating[12,14,34,35].

Given the primacy of mating to reproduction, neural circuits must also generate a desire to mate. Such sexual motivation promotes mate-seeking, and male rodents will endure foot-shocks to gain access to females[36,37]. Dopaminergic pathways modulate sexual desire or drive, but how these influence circuits that promote mating is poorly understood[38–40].

Sexual behavior is rewarding, presumably as a means to enhance reproduction, but how neural circuits implement this is elusive. Moreover, it is unclear whether such neural pathways are specific to mating-related reward. Classic neuronal self-stimulation studies have suggested the presence of a “pleasure center” for mating in the brain[41]. Both the identity of this pleasure center and how it relates to the mating circuit remain to be determined.

Here we use a combination of molecular genetics, neuronal activity monitoring, and functional studies to address these long-standing issues. Our studies reveal a molecularly-specified, developmentally-wired neural circuit that distinguishes between sexes, is innervated by chemosensory pathways, implements motor programs for mating but not aggression, and governs sexual drive and reward.

RESULTS

Male BNSTpr^{Tac1} neurons are preferentially activated by females and sufficient for mating

Estrogen receptor alpha (Esr1 or ERα)-expressing BNSTpr (BNSTpr^{Esr1}) neurons consist of molecularly distinct cells as defined by snRNAseq[9] (Fig. 1A). Male aromatase-expressing BNSTpr^{Esr1} (BNSTpr^{Aro}) neurons are differentially activated by females and required to distinguish between sexes[10]. Of all BNSTpr^{Esr1} neurons, only the transcriptomically-defined BNSTpr^{Tac1} cell type (a subset of BNSTpr^{Aro} neurons) is essential to distinguish between sexes[9]. Furthermore, inhibition of male BNSTpr^{Tac1} but not other BNSTpr^{Esr1} neurons essentially abrogates mating and aggression. We tested whether BNSTpr^{Tac1} neurons would also be differentially activated by females, using fiber photometry in sexually naive Tac1^{Cre} males[42] (Fig. 1B-E, S1A-M; Table S1). Sexually naive males distinguish between female

and male cues[9,10] even though they do not reliably emit courtship ultrasonic vocalizations (USVs) (Table S2). Accordingly, BNSTpr^{Tac1} neurons were more responsive to female urine (Fig. 1B-E). Similarly, they were more responsive to a female (Fig. S1A-E), activated during mating, and quiescent during aggression (Fig. S1G-M). Thus, the activity of BNSTpr^{Tac1} neurons of sexually naive males distinguishes between sexes and reflects mating.

To understand activation of BNSTpr^{Tac1} neurons at single cell resolution, we imaged these cells from sexually naive males with a miniscope (Inscopix) while presenting pheromonal cues (Fig. 1F-N, S1N-O; Table S1). Many cells (~42%) were activated by female or both female and male cues, whereas few (~3%) were activated solely by male cues (Fig. 1H-L). Of cells co-activated by female and male urine, most showed larger activation with female cues (Fig. 1M-N). BNSTpr^{Tac1} neurons therefore distinguish between sexes in two ways: female cues activate more of these cells and at higher levels (Fig. 1L-N, S1O). A recent study reported that sex recognition by BNSTpr^{Esr1} cells resulted solely from more cells being activated by female cues[19]. This difference likely reflects the fact that we were imaging the transcriptomically-defined cell type (BNSTpr^{Tac1}) essential for male-typical social behaviors rather than the larger BNSTpr^{Esr1} population whose function(s) remain unknown.

The activity of male BNSTpr^{Aro} and BNSTpr^{Tac1} neurons distinguishes between sexes early during the encounter, with higher and longer activation by females[10] (Fig. 1B-N, S1A-E) (BNSTpr^{Tac1} neurons, time for GCaMP6s signal to return to baseline: female 90 ± 7.3 s; male 65.8 ± 8.5 s; n = 6; p = 0.009). Optogenetic activation of male BNSTpr^{Aro} neurons for the first 90 s of a social encounter inhibits aggression and promotes mating with a male without altering mating with a female[10], and these phenotypes were also observed by similar activation of male BNSTpr^{Tac1} neurons (Fig. 1O-V, S1P-S; Tables S1, S3). As with BNSTpr^{Aro} neurons[10], activation of BNSTpr^{Tac1} neurons did not immediately trigger mating with males; rather, mating probability, mating latency, and the number of mounts with the male were indistinguishable from those observed in mating with females without optogenetic activation (Mating probability: with female, 0.6; with male, 0.8; p = 0.999; Mating latency: with female, 600 ± 72.5 s; with male, 496.8 ± 79.1 s; p = 0.461; Mount #: with female, 8.5 ± 2.5; with male, 5.8 ± 1.1; p = 0.291) (Fig. 1P,T-V, S1Q,R). As with BNSTpr^{Aro} neurons[10], intermittent activation of BNSTpr^{Tac1} neurons did not elicit hypersexual behavior with females (Fig. S1T-V) (Mating latency: laser on, 724.8 ± 279.1 s; laser off, 859.9 ± 263.2 s; n = 5; p = 0.758; Mount #: laser on, 19.8 ± 2.1; laser off, 16 ± 5; n = 5; p = 0.476).

Together, activation of BNSTpr^{Tac1} neurons induces males to treat males as females, and it does not promote hypersexual behaviors with females. These findings support the notion[9,10] that activity of BNSTpr^{Tac1} neurons does not enhance sexual motivation but rather reports the presence of a female.

The projection of BNSTpr^{Tac1} to POA^{Tacr1} neurons governs mating but not aggression

To identify postsynaptic targets of BNSTpr^{Tac1} neurons, we expressed synaptophysin-mRuby (Syp:mRuby) in these cells. The largest zone of mRuby+ innervation was the POA (Fig. 2A-B), which regulates male mating[17,18,43,44]. Expressing a reporter in the POA

of *Tacr1*^{Cre} males[45] revealed putative postsynaptic partners of BNSTpr^{Tac1} cells (Fig. 2C-D). Indeed, using an EGFP-encoding monosynaptic rabies vector[46,47] we observed starter POA^{Tacr1} neurons (TVA+, EGFP+) in the POA and presynaptic neurons (TVA–, EGFP+) within the BNSTpr (Fig. 2E-F). Most (~93%) BNSTpr^{EGFP} cells expressed Tac1, and ~45% of BNSTpr^{Tac1} neurons were EGFP+ (Fig. 2G-I). Taken together (Fig. 1A, 2H-I), BNSTpr^{Tac1} cells represent the major presynaptic input from BNSTpr to POA^{Tacr1} neurons.

We optogenetically tested whether BNSTpr^{Tac1}→POA^{Tacr1} projections regulated mating or aggression (Fig. 2J; Table S1). Activation of these projections at the start of a social encounter suppressed aggression and promoted mating with males without altering mating with females (Fig. 2K-L, S2A-H; Table S3). This recapitulates the phenotype obtained by activation of BNSTpr^{Tac1} soma, indicating that BNSTpr^{Tac1}→POA^{Tacr1} projections convey the presence of a mate. Conversely, inhibiting these projections with the optogenetic actuator parapinopsin (PPO)[48] suppressed mating, reducing mating probability ~6-fold and mount number >8-fold (Fig. 2M-O, S2I-N; Tables S1, S3). By contrast, such inhibition did not discernibly alter aggressive displays toward a male (Fig. 2P-Q, S2O-S). Together, BNSTpr^{Tac1}→POA^{Tacr1} projections are necessary and sufficient for male mating but not aggression.

POA^{Tacr1} neurons are activated during and critical for mating but not aggression

The foregoing findings suggest that POA^{Tacr1} neurons regulate mating specifically. Indeed, virtually all POA^{Tacr1} neurons express Esr1 (Fig. S3A-D), and POA^{Esr1} neurons are active during and critical for male social behaviors, including mating[17,18]. Fiber photometry imaging of sexually naive males interacting with a female showed that POA^{Tacr1} neurons were activated during anogenital chemoinvestigation (sniffing), mounting, and intromission (penetration) (Fig. 3A-C, S3E-I; Table S1), whereas they were not activated when sniffing or attacking a male (Fig. 3D-F). We next tested whether experimentally activating male POA^{Tacr1} neurons regulated mating. Optogenetic activation of POA^{Tacr1} cells reduced mating latency and elicited time-locked mating (Fig. 3G-J; Tables S1, S3), with >6-fold more mating bouts during light epochs (15 s on and 45 s off) (Fig. S3J-L). Activation of POA^{Tacr1} neurons suppressed aggression and elicited time-locked mating attempts toward males (Fig. 3K-N, S3M; Movie S1). Together, activating male POA^{Tacr1} neurons drives mating at the expense of aggression.

Activating POA neurons elicits USVs, but the molecular identity of these cells remains to be fully defined[49,50]. Optogenetic activation of male POA^{Tacr1} cells induced time-locked USVs, but no mounting-type displays (0/4 males), in sexually naive males in the absence of a conspecific (Fig. S3N-Q; Tables S1, S3). Together, POA^{Tacr1} neurons trigger USVs but not mating routines in naive, isolated males.

The alacrity with which males mated upon activation of POA^{Tacr1} neurons prompted us to test whether they would mate with inanimate objects (Movie S1). Optogenetic activation of male POA^{Tacr1} neurons increased investigation of a beaker, wooden block, and a 5 mL Eppendorf tube without inducing mounting (Fig. 3O-R; Tables S1, S4). Strikingly, outfitting the tube with the tail-end of a toy mouse induced mounting during light epochs (Fig. 3S; Table S4). Activation of male POA^{Tacr1} neurons progressively increased mounting

towards a toy mouse, another male, and a sexually unreceptive female. (Fig. 3T-V; Table S4; Movie S1). Such mounts were largely directed toward the tail-end of the object or mouse, indicating that, in conjunction with activation of POA^{Tacr1} neurons, this feature was a releaser stimulus for mating. More broadly, activation of these cells induces time-locked mating with females and atypical targets, including ersatz mice.

We tested whether activity of POA^{Tacr1} neurons was essential for mating. Optogenetic inhibition of POA^{Tacr1} neurons abrogated mating with females (0/11 males mounted), without altering sniffing (Fig. 4A-C, S3R-T; Tables S1, S3). POA^{Tacr1} neurons are also activated upon transitioning from mount to intromission, suggesting that this activity regulates intromission. Indeed, we observed that mount-triggered inhibition reduced intromission >10-fold, and across all mounts, intromission probability dropped from 0.82 to 0.07 (Fig. 4D-F). Male POA^{Tacr1} neurons show no discernible activation during aggression (Fig. 3D-F), and correspondingly, their inhibition did not alter fighting (Fig. 4G-K, S3U). Taken together, POA^{Tacr1} neurons are active during mating, and their activity is necessary and sufficient for mating but not aggression.

POA^{Tacr1} neurons function downstream of BNSTpr^{Tac1} neurons in promoting male mating

Our findings suggest that male POA^{Tacr1} neurons function downstream of BNSTpr^{Tac1} neurons in the mating circuit. We tested this with neural circuit epistasis studies using intersectional genetics. In the absence of a *Tac1^{Flpo}* line, we employed the *Esr1^{Flpo}* strain[9] to access the BNSTpr^{Tac1} population, the only BNSTpr^{Esr1} cell type essential for male mating[9,10]. We expressed the inhibitory chemogenetic actuator DREADDi[51] in POA^{Tacr1} neurons and ChR2 in BNSTpr^{Esr1} neurons of *Esr1^{Flpo};Tacr1^{Cre}* males (Fig. 4L, S4A-C; Tables S1, S3). As expected, males did not mate with females when given the DREADD ligand CNO but territorial aggression or other behaviors were unaffected (Fig. 4M-N, S4D-E, H-L); in separate control experiments, optogenetic activation of BNSTpr^{Esr1} neurons, similar to activating BNSTpr^{Tac1} neurons, induced mating toward males (Fig. 1O-R, S4F-G). However, activation of BNSTpr^{Esr1} neurons while inhibiting POA^{Tacr1} neurons did not elicit male sexual behavior (Fig. 4O-P, S4M-P). Together, the mating-promoting effect of BNSTpr^{Esr1} neurons is upstream of POA^{Tacr1} neurons.

We tested whether POA^{Tacr1} neurons were functionally downstream of BNSTpr^{Esr1} neurons. Accordingly, we expressed DREADDi and ChR2 in male BNSTpr^{Esr1} and POA^{Tacr1} neurons, respectively (Fig. 4Q, S4Q-S; Tables S1, S3). As expected, light activated POA^{Tacr1} neurons and, in separate tests, CNO inhibited males from mating with females (Fig. 4R-S, S4S-V). Activating POA^{Tacr1} neurons while inhibiting BNSTpr^{Esr1} neurons elicited mating with females, with a >9-fold increase in mating probability (Fig. 4T-U, S4W-Y). Altogether, POA^{Tacr1} neurons are anatomically and functionally downstream of BNSTpr^{Tac1} neurons, which are a subset of BNSTpr^{Esr1} neurons.

Substance P released by male BNSTpr^{Tac1} neurons acts on POA^{Tacr1} neurons to promote mating

Substance P, encoded by *Tac1*, is expressed in the BNSTpr and, among tachykinin neuropeptides, it is the cognate ligand for the receptor Tacr1[52–54], which is important for

male mating[55,56]. Accordingly, most *Tac1*$^{-/-}$ males did not even initiate mating (*Tac1*$^{-/-}$, 1/7 mated; WT, 5/6 mated; p = 0.029). Substance P and Tacr1 are expressed widely and regulate diverse behaviors beyond social interactions[52–54], and it is unclear where they act to regulate mating. We hypothesized that BNSTpr^{Tac1} and POA^{Tacr1} neurons use this neuropeptide-receptor pair to regulate mating.

We first recorded from POA^{Tacr1} neurons in slices to test this hypothesis. Although Substance P can increase excitability of other neurons[57,58], it did not change the firing rate of POA^{Tacr1} neurons (S5A-D). We next tested whether Substance P enhanced excitatory input onto POA^{Tacr1} neurons. Similar to its effects in other neurons[59–61], Substance P (50 nM) induced long-term potentiation (LTP) of evoked excitatory postsynaptic potentials (EPSPs) in POA^{Tacr1} neurons, and this LTP was abolished by L-703,606, a Tacr1 antagonist[56,62] (Fig. 5A-D). Furthermore, optogenetic activation of BNSTpr projections also induced LTP in POA^{Tacr1} neurons in a Tacr1-dependent manner (Fig. 5E-H). Thus, Substance P released by BNSTpr^{Tac1} neurons signals through Tacr1 to induce excitatory LTP in POA^{Tacr1} neurons.

Given that BNSTpr^{Tac1} neurons are GABAergic[9], we wondered how Substance P induced LTP in POA^{Tacr1} neurons. Optogenetic activation of BNSTpr projections in the POA inhibited firing of POA^{Tacr1} neurons acutely without perdurant effects (Fig. S5E-H). As standard in the field[63–65], our LTP recordings included the GABA-A blocker picrotoxin (Fig. 5E-H). However, we also observed robust Tacr1-dependent LTP without picrotoxin (Fig. S5I-K). Thus, activation of GABAergic BNSTpr^{Tac1} neurons initially inhibits but ultimately elicits Tacr1-dependent excitatory LTP in POA^{Tacr1} neurons.

Male BNSTpr^{Tac1} neurons are activated for ~90 s when first encountering a female whereas mating ensues 10–15 min later (Fig. S1A-E). Sustained activity of neuromodulatory neurons is thought to elicit presynaptic release of neuropeptides[66]. We hypothesized that this ~90 s activation of BNSTpr^{Tac1} neurons would release Substance P and potentiate excitatory transmission onto POA^{Tacr1} neurons *in vivo*. We observed a Tacr1-dependent, ~1.6-fold increase in the ratio of evoked AMPA and NMDA receptor-mediated currents (AMPA/NMDA ratio) in POA^{Tacr1} neurons of virgin males interacting with females prior to mounting (Fig. 5I-M). The paired-pulse ratio in POA^{Tacr1} neurons was not discernibly altered (Fig. S5L-P). Together, encountering a female elicits a Substance P-induced enhancement of excitatory transmission onto POA^{Tacr1} neurons that precedes mating.

We wondered if the time-course of this Substance P-induced plasticity of POA^{Tacr1} neurons *in vivo* provided a timer mechanism for male mating initiation. If so, Substance P should bidirectionally regulate mating onset. Substance P infusion into the POA reduced male mating latency by 2.4-fold (Fig. 5N-P, S6A-C). Conversely, L-703,606 increased mating latency such that most males did not mate (Fig. 5Q-S). Importantly, aggressive and locomotor behaviors appeared unchanged (Fig. S6D-J). Our findings therefore indicate that Substance P-induced LTP of POA^{Tacr1} neurons provides a molecular timer for male mating onset.

We tested whether male mating induced by POA^{Tacr1} neurons is downstream of Substance P signaling from BNSTpr^{Tac1} projections. We optogenetically activated these projections or POA^{Tacr1} neurons in separate experimental cohorts ± L-703,606 (Fig. 5T,U,W, S6O; Tables S1, S3). We delivered L-703,606 systemically because the optogenetic setup precluded delivery to the POA. L-703,606 inhibited mating despite activation of BNSTpr^{Tac1}→POA projections, whereas activation of POA^{Tacr1} neurons bypassed this pharmacologically-enforced mating block (Fig. 5V,X, S6K-N, P-U). Taken together, Substance P released by BNSTpr^{Tac1} neurons potentiates activation of POA^{Tacr1} neurons in a Tacr1-dependent manner to initiate male mating.

Male POA^{Tacr1} neurons regulate sexual drive and reward

Males lose mating drive following ejaculation and enter a refractory period that lasts ~5 days in C57BL/6J mice[67,68] (Data S1). Activation of hypothalamic dopaminergic AVPV/PVpoTH neurons restores mating, albeit with variable delays, during the refractory period[39]. This effect depends on dopamine receptor DRD1 that is thought to be widely expressed in POA^{Esr1} neurons[39]. Non-targeted activation of rat POA neurons also shortens the refractory period[69]. RNAseq studies show that DRD1 is expressed only in a small subset of Esr1+, Tacr1–, POA neurons[9,70]. Given that Tacr1 activation, like DRD1 activation, elevates intracellular cAMP[52] and optogenetic activation of POA^{Tacr1} neurons drives time-locked mating, we tested whether activation of these cells restored mating drive. Optogenetic activation of POA^{Tacr1} neurons immediately following ejaculation triggered time-locked mating and many males ejaculated again (Fig. 6A-D, S7A-C; Tables S1, S3; Movie S2). Thus, activation of POA^{Tacr1} neurons restores mating drive and shortens the ~5 day refractory period to ~1 s.

The hypothalamus contains sites whose activation elicits neuronal self-stimulation[41,71–75]. Given that mating is rewarding, we wondered whether POA^{Tacr1} neurons encoded mating-related reward. We developed a social place preference (SPP) paradigm in which males displayed preference for an area housing a mating-inaccessible female (Fig. 6E-G; Tables S1, S3). Area-specific optogenetic activation of POA^{Tacr1} neurons strengthened preference for that area regardless of the presence of a female (Fig. 6F,H-I, S7D-E). Together, activation of male POA^{Tacr1} neurons is strongly reinforcing and even overrides the attraction to females.

We next tested whether males would optogenetically self-stimulate POA^{Tacr1} neurons by nose-poking to a light-delivering (active) port in a 2-port chamber (Fig. 6J; Tables S1, S3). Males self-stimulated POA^{Tacr1} neurons, with sexually experienced males nose-poking more than naive males (Fig. 6J-L, S7F-G; Movie S2). In summary, POA^{Tacr1} neurons constitute a molecularly-defined mating center that encodes reward that is enhanced by sexual experience.

Activation of POA^{Tacr1} neurons is rewarding, and we wondered whether inhibition of these cells would be aversive. Optogenetic inhibition of these cells however did not alter males' preference for the female-occupied area in the SPP paradigm, showing that inhibiting POA^{Tacr1} cells suppresses mating but does not lead to avoidance of females (Fig. 6M-N, S7H-J; Tables S1, S3). Similarly, inhibition of POA^{Tacr1} neurons did not discernibly alter

consumption of sucrose-sweetened water, a fluid innately attractive to mice[76] (Fig. 6O-P). Thus, inhibiting these neurons does not induce general anhedonia. Altogether, male POA^{Tacr1} neurons govern sexual drive, reward, and displays.

POA^{Tacr1} neurons act independent of dopaminergic AVPV/PVpoTH neurons to modulate sexual drive and reward

In contrast to other neuronal populations[39,77], activation of POA^{Tacr1} neurons immediately restores mating during the refractory period. We tested whether POA^{Tacr1} cells are functionally downstream of one such population, the AVPV/PVpoTH neurons[39], in regulating mating drive. Local delivery of 6-hydroxy DOPA (6OHDA), a dopaminergic neuron-specific toxin, reduced AVPV/PVpoTH neuron number ~3-fold, with a smaller diminution in TH neurons in the ventral tegmental area (VTA), presumably via diffusion of 6OHDA (Fig. 7A, S8A-B; Tables S1, S3). This ablation did not discernibly alter male mating, and furthermore optogenetic activation of POA^{Tacr1} neurons immediately restored mating following ejaculation in all of these males (Fig. 7C-D, S8C-D). Although dopamine signaling is considered central to behavioral reinforcement[78], optogenetic activation of POA^{Tacr1} cells guided place preference and induced self-stimulation in these males (Fig. 7E-F). Our findings indicate that POA^{Tacr1} neurons are functionally downstream of AVPV/PVpoTH neurons in regulating sexual drive. Further, POA^{Tacr1} neurons reinforce behavior independent of any dopamine released by AVPV/PVpoTH neurons.

The BNSTpr^{Tac1}→POA^{Tacr1} circuit directly links to centers for sensory input, motor output, and reward

We sought to place the BNSTpr^{Tac1}→POA^{Tacr1} pathway in context of an anatomical framework that endows male mating with its defining features: pheromonal control, reward, and motor displays. We used monosynaptic rabies to determine if BNSTpr^{Tac1} or POA^{Tacr1} neurons were innervated by main or accessory olfactory bulbs (MOB and AOB), which receive pheromonal input from the nose[79]. We observed presynaptic neurons exclusively in the AOB and only when BNSTpr^{Tac1} neurons comprised the starter population (Fig. S8E-N). This is in agreement with work showing that only the BNST receives olfactory bulb input[79–81], and we further show that AOB innervates BNSTpr^{Tac1} neurons. Together, pheromonal input converges onto BNSTpr^{Tac1} neurons, whose activity distinguishes between sexes in a pheromone sensing-dependent manner[10].

To understand how POA^{Tacr1} neurons drive mating and reinforcement, we traced their projections using Syp:mRuby. In addition to other targets, these neurons projected to the periaqueductal gray (PAG) and VTA, centers that gate motor output and reward, respectively (Fig. S8O-Q). We optogenetically activated PAG and VTA projections of POA^{Tacr1} neurons in separate experimental cohorts (Fig. 7G,L; Tables S1, S3). Surprisingly, activation of either VTA or PAG projections elicited nose-pokes to the active port and mounting toward both sexes (Fig. 7H-J, M-O, S9A-D). Activation of these projections elicited comparable nose-pokes to the active port (PAG projections, 238 ± 25, and VTA, 284 ± 35.3; n = 7 each; $p > 0.99$). By contrast, mounting induced by activation of VTA projections did not progress to intromissions whereas activation of PAG projections led to mounting and intromission (Fig. 7K,P). Together, activation of VTA and PAG projections of POA^{Tacr1} neurons elicits

self-stimulation, and VTA projections can drive mounting whereas PAG projections drive both mounting and intromission.

The foregoing findings could reflect antidromic activation of POA^{Tacr1} soma upon activating their projections to the VTA or PAG. We delivered differently-labeled cholera toxin B[82] (CTB), a retrograde tracer, to the VTA and PAG to test whether POA^{Tacr1} neurons collateralize to both targets. We found that ~50% of VTA-projecting POA^{Tacr1} cells also projected to the PAG and vice versa (Data S1). We have likely underestimated the extent of collateralization because the rostrocaudal extent (>1 mm) of the VTA and PAG precluded comprehensive labeling of POA^{Tacr1} projections. Given such collateralization of projections, we eliminated antidromic activation of POA^{Tacr1} soma with locally-delivered tetrodotoxin (TTX[83]) and optogenetically activated these projections. Activation of projections to either the VTA or PAG induced self-stimulation and mating displays, in a manner indistinguishable from males administered vehicle instead of TTX (Fig. S9E-J). We conclude that projections of POA^{Tacr1} neurons to the VTA or PAG regulate mating behaviors and reward-related displays.

Mesolimbic dopamine signaling is considered a *sine qua non* for reward-related responses[38,40,78,84]. We therefore tested whether activation of POA^{Tacr1} neurons would elicit dopamine release in the nucleus accumbens (NAc), a reward hub[78]. The anatomical proximity of the POA and NAc precluded concurrent POA^{Tacr1} soma activation and dopamine imaging. We therefore optogenetically activated POA^{Tacr1} projections to the VTA, which sends massive projections to the NAc[78,85], and imaged dopamine release in the NAc with $GRAB_{DA}$[86]. This experiment revealed a time-locked increase in $GRAB_{DA}$ signal (Fig. 7Q-T, S9K-P; Tables S1, S3). This signal was neither perdurant nor rapidly diminishing across activation epochs, thereby suggesting a cellular mechanism whereby mice repeatedly self-stimulate these cells to obtain reward (Fig. 6J-L). More generally, our findings indicate that the rewarding aspect of POA^{Tacr1} activation involves mesolimbic dopamine signaling.

DISCUSSION

We have identified a neural circuit for innate male sexual behavior (Fig. 7U). This circuit enables recognition of potential mates and motor displays of mating, rejuvenates sexual drive, and makes mating rewarding. Moreover, our findings show that the brain employs distinct neural circuits to generate male mating and aggression.

A male mating circuit

Male sexual behavior is regulated by a motivational state or drive – libido in humans – that enables even sexually naive animals to mate. It is also rewarding in the sense that humans self-report it to be pleasurable and animals seek to mate repeatedly. The neural circuit we have uncovered incorporates these and other essential features of male sexual behavior. It receives sensory input, recognizes potential mates, elicits mating even in sexually naive males, governs sexual drive, and its activation is rewarding. $BNSTpr^{Aro}$ neurons, of which $BNSTpr^{Tac1}$ neurons are a subset, exhibit extreme sexual dimorphism in that they elicit male sexual behavior only in males[9,10]. Together, this suggests a mechanism whereby the neural circuit we have described preferentially elicits male-typical mating displays in males.

BNSTpr^{Tac1} neurons of sexually naive males provide a neuronal activity signature of sex recognition, a signature predictive of subsequent mating with females and fighting with males. USVs have been used as a surrogate for sex recognition and to categorize male mating as either sexual or aggressive in nature[18,19]. However, only sexually experienced males emit USVs differentially and reliably to females, and these USVs are governed by context, genetic background, and prior experience, including with males[87–91]. Thus, there are confounds to using USV to categorize male mating as sexual or aggressive in intent or as a surrogate for sex recognition. It may be more informative to label male mating agnostically with motor routines shared across species and to use the activity signature of BNSTpr^{Tac1} neurons as a measure of sex recognition.

It has been challenging to pinpoint neurons that regulate male mating but not aggression. This has led to a model wherein all innate social behaviors are co-regulated by several brain regions that comprise a “social behavior network”[24]. This network is proposed to be a fully connected, single layer system, with individual behaviors arising as an emergent output. However, we find that there are developmentally-patterned asymmetries in the neuronal encoding of male mating. BNSTpr^{Tac1}, but not POA^{Tacr1}, neurons receive pheromonal input and disabling this input disables BNSTpr neurons from distinguishing between sexes[10]. Our epistasis studies further establish an upstream-downstream relationship between BNSTpr^{Tac1} and POA^{Tacr1} neurons. Recent studies have identified additional centers that regulate male mating and aggression and could be considered to comprise an extended social behavior network[16,21,92,93]. Nevertheless, information flow even within this extended network cannot compensate for disabling POA^{Tacr1} neurons. Thus, in contrast to a social behavior network, we find directional transfer of information in a neural circuit that drives male mating but not another innate social behavior, aggression.

POA^{Tacr1} neurons do not merely relay information from BNSTpr^{Tac1} neurons. First, they regulate mating and not aggression. They also encode a timer mechanism that delays mating onset following sex recognition. This lag in mating onset lasts several minutes whereas male BNSTpr^{Tac1} neurons recognize females within seconds. The Substance P-potentiated excitatory transmission onto POA^{Tacr1} neurons, which occurs over several minutes, provides a timer mechanism for the delay in mating onset. In agreement with this notion, experimental activation of POA^{Tacr1} but not BNSTpr^{Tac1} neurons bypasses this delay to trigger mating. More broadly, a biological timer may have evolved to enable animals to assess other contingencies such as proximity of predators prior to mating.

POA^{Tacr1} projections to the VTA and PAG drive male mating, reinforcement, and immediate recovery from the refractory period (PAG, 7/7 males; VTA, 1/1 male). There may exist POA^{Tacr1} neurons projecting uniquely to these targets and regulating subsets of these behavioral features. Alternatively, simultaneous broadcasting of these features may be an integral property of the mating circuit that links behavior and internal states. Such a circuit model differs from the one for parenting[94], in which POA^{Gal} neurons broadcast behavioral features to different brain regions to govern parenting. Together, different innate social behaviors governed by the POA may utilize distinct circuit architectures, presumably reflecting unique evolutionary histories or needs.

Sexual drive and reward

Animals desire to mate and to do so repeatedly. Male mating is appetitive or rewarding and associated with a drive that promotes mating even in sexually naive animals[3,36,37,95]. So-called pleasure centers in the brain also elicit self-stimulation[41,71,72,96]. However, neurons whose activity is self-reinforcing and promotes male mating were unknown. In principle, sexual reward and displays could be encoded by distinct centers. However, the activity of POA^{Tacr1} neurons triggers time-locked mating and drives self-stimulation of these cells, which likely entails mesolimbic dopamine signaling. Thus, the same neuronal population drives mating and reward, providing an intimate cellular link between mating and its hedonic value. These neurons are not essential for rewarding prosocial behaviors such as approach[97–99], aggression, or for reward associated with non-social behaviors. Thus, POA^{Tacr1} neurons may be exclusively purposed for male mating and its associated reward.

Studies of drive mechanisms for drinking and feeding have provided two modes of operation that enable animals to satisfy needs[100–106]. Aversive drives motivate animals to perform behaviors that enable return to a homeostatic setpoint. Other drives regulate behavior bidirectionally such that activation of key neurons is rewarding whereas their inhibition is aversive. By contrast, activation of POA^{Tacr1} neurons is rewarding whereas their inhibition is not aversive, thereby identifying another drive mechanism to satisfy innate needs. More broadly, POA^{Tacr1} cells represent a molecularly-identified neuronal subset that is active during behavior, is necessary and sufficient for the behavior, drives it in a time-locked manner, regulates behavioral drive, and is rewarding.

POA^{Tacr1} neurons provide an entry point to understand sexual drive. The male primate POA is active during mating, and its activation can promote mating[107–109]. This close concordance between male primate and rodent sexual behavior suggests that this region also regulates libido in men. Drugs that help with erectile dysfunction[110] are ineffective for loss of libido. POA^{Tacr1} neurons may offer a therapeutic target to modulate libido in humans.

Limitations of the study

Response profiles of $BNSTpr^{Tac1}$ neurons were obtained using undiluted urine, and these could change when different amounts or dilutions of urine are used. Rabies vectors exhibit tropism, and we cannot exclude the possibility that some presynaptic neuronal populations were not labeled. Substance P signaling modulates mating latency and induces LTP onto POA^{Tacr1} neurons. Further studies are needed to directly link LTP to mating latency and determine whether Substance P utilizes other signaling pathways to regulate latency. We used systemic antagonism of Tacr1 for some studies, and in future studies it will be important to test whether Tacr1 functions in POA^{Tacr1} neurons to regulate mating. The circuit or synaptic mechanisms whereby GABAergic POA^{Tacr1} neurons govern behavioral and physiological outcomes remain to be determined. We imagine that projections of $BNSTpr^{Tac1}$ and POA^{Tacr1} neurons that we have not examined in this study may also modulate the social interactions that we have assayed as well as other behaviors. GCaMP6s fluorescence is a surrogate for neuronal firing, and *in vivo* voltage recordings during social interactions will be important to reveal the firing patterns within the mating circuit we have identified.

STAR METHODS

Resource Availability

Lead contact—Further information and requests for resources and reagents should be directed to and will be fulfilled upon reasonable request by the lead contact, Dr. Nirao M. Shah (nirao@stanford.edu).

Materials availability—This study did not generate new unique reagents.

Data and code availability

- Data reported in this paper will be shared by the lead contact upon request.
- All scripts used in this manuscript are available from the lead contact upon reasonable request.
- Any additional information required to reanalyze data reported in this paper is available from the lead contact upon request.

EXPERIMENTAL MODEL AND SUBJECT DETAILS

Animals—Adult mice 10–24 weeks of age were used for all studies. All mice were bred in our colony (*Tac1*^{Cre}*, Tacr1*^{Cre}*, Tac1 null, Esr1*^{Flpo})[9,42,45,112] or purchased from Jax (*C57BL/6J*, used as WT resident males and stimulus females in mating assays) and Charles River (*BALB/c*, used as WT intruder males). Mice were housed under a reverse 12:12 hour light:dark cycle (lights off at 1pm) with controlled air, temperature, and humidity, and food and water were provided *ad libitum* unless otherwise mentioned. Mice were group housed by sex after weaning at 3 weeks of age and were therefore sexually naive prior to initiation of behavioral testing. All animal studies were done in compliance with Institutional Animal Care and Use Committee guidelines and protocols approved by Stanford University's Administrative Panel on Laboratory Animal Care and Administrative Panel of Biosafety.

Viruses—AAV-hSyn-DIO-GCaMP6s (serotype 1), AAV-EF1α-DIO-PPO:Venus (serotype 9), AAV-EF1α-DIO-hChR2(H134R)-EYFP (serotype 1), AAV-hSyn-hChR2(H134R)-EYFP (serotype 1), AAV-CAG-DIO-EGFP (serotype 1), and AAV-CAG-DIO-tdTomato (serotype 1) were purchased from Addgene. AAV-EF1α-DIO-hChR2(H134R):mCherry (serotype 2), AAV-EF1α-DIO-eNpHR3.0:mCherry (serotype 2), AAV-EF1α-DIO-mCherry (serotype 2), AAV-EF1α-DIO-hM4Di:mCherry (serotype DJ, encoding DREADDi), AAV-EF1α-fDIO-hM4Di:mCherry (serotype DJ, encoding DREADDi), and AAV-EF1a-fDIO-hChR2(H134R):EYFP (serotype DJ) were purchased from UNC Vector Core. AAV-hSyn-DIO-mGFP-2A-Synaptophysin:mRuby (serotype DJ), and AAV-DIO-TVA:mCherry-2A-oG (serotype 8.2) were custom packaged by Virovek (Hayward, CA). EnvA G-deleted Rabies-EGFP was purchased from Salk Institute. Cholera Toxin Subunit B (CTB), Alexa Fluor 555 and 647 conjugates were purchased from ThermoFisher Scientific. AAV-hSyn-GRAB_DA2m (serotype 9) was purchased from Addgene. All virus titers were > 10^{12} genomic copies/mL.

METHOD DETAILS

Stereotaxic surgeries—Viruses were delivered into brains of male mice at 10–16 weeks of age, using a Kopf stereotaxic alignment system (model 1900), as described previously[10]. Viruses were injected into empirically determined coordinates for the BNSTpr and POA (BNSTpr: ±0.85 mm mediolateral (ML), −0.20 mm anteroposterior (AP), and −4.30 mm dorsoventral (DV) relative to bregma; POA: ±0.60 mm ML, +0.05 mm AP, and −5.20 mm DV). For fiber photometry and miniscope studies, 0.5 μl of virus was injected unilaterally (counterbalanced for injections into left or right hemisphere across animals), and for all circuit mapping and functional manipulation studies, 0.5 μl of virus was injected bilaterally. Viruses were infused at a rate of 100 nl/min using a syringe pump (Harvard Apparatus), and the needle was left for an additional 5 min and withdrawn at 1 min/mm.

For fiber photometry and optogenetic manipulation studies, following viral injection during the same surgery, mice were implanted with an optic fiber (0.5 NA, 400 μm diameter and 0.39 NA, 200 μm diameter, respectively; RWD Life Sciences) placed 0.5 mm above the viral injection site of either the BNSTpr, POA, or NAc, depending upon the functional manipulation. For the POA^{Tacr1} projection activation experiments, optic fibers were placed at empirically determined coordinates for the VTA and PAG (VTA: ±0.50 mm ML, −2.92 mm AP, and −4.50 mm DV; PAG: ±0.50 mm ML, −4.60 mm AP, and −2.50 mm DV). For POA^{Tacr1} projection activation with concurrent $GRAB_{DA}$ photometry experiments, an activating optic fiber was placed over the VTA and the recording optic fiber was placed over the ipsilateral NAc (±1.20 mm ML, +1.2 mm AP, and −4.20 mm DV). An additional activating optic fiber was placed over the contralateral POA for USV experiments. For local POA infusion of Tacr1 antagonist studies, mice were implanted with dual cannulas (RWD Life Sciences) placed above the POA (±0.60 mm ML, +0.05 mm AP, and −4.70 mm DV). For miniscope imaging studies, a 0.6 mm x 7.3 mm (diameter x length) GRIN lens (Inscopix) was implanted 3 weeks after viral injection. The GRIN lens was connected to a miniscope imaging system (nVista, Inscopix), lowered at 0.5 mm/min while monitoring fluorescence, and placed between 150 and 250 μm dorsal to the coordinates used for viral delivery. The GRIN lens was capped with a small piece of parafilm and silicon adhesive (Kwik-Sil, WPI) prior to closing the skin incision. The silicon cover was removed 14 days after GRIN lens implantation and a baseplate (Inscopix) was installed above the GRIN lens. The baseplate was connected to the miniscope, lowered until clear cellular morphology was detected across the imaging plane, anchored to the skull with adhesive, and covered with a baseplate cover (Inscopix). Cannulas, GRIN lens, and baseplates were secured to the skull using adhesive dental cement (C&B Metabond, Parkell). Following surgery, mice were allowed to recover individually over a heat pad and then returned to their home cages.

For monosynaptic rabies vector-based trans-synaptic labeling, we first delivered an AAV (0.4 μL) encoding Cre-dependent TVA and rabies G glycoprotein to the POA ($Tacr1^{Cre}$ males) or BNST ($Tac1^{Cre}$ males). Two weeks following AAV delivery, we delivered an EGFP-encoding rabies vector (0.2 μL) to the same regions. We euthanized males 1 week following delivery of rabies vector and performed immunolabeling for TVA and EGFP to visualize presynaptic cells. For CTB labeling of EGFP+ POA^{Tacr1} projections to the VTA and PAG, 0.2 μL of CTB labeled with different fluorophores was delivered to each of these

projection fields. Males were euthanized one week following CTB delivery and processed for histology.

Histology—We confirmed expression of all virally delivered genes in all experimental animals using previously published procedures[9,10,12,113]. Mice were anesthetized with 2.5% avertin and perfused with HBS followed by 4% paraformaldehyde (PFA). Brains were dissected, post-fixed in 4% PFA overnight, sectioned at 65μm thickness with a vibratome (Leica VT1000S), and immunolabeled and counter-stained with DAPI (0.2 μg/mL). Primary antisera were sheep anti-GFP (BioRad; 1:2000), rat anti-RFP (Chromotek; 1:2000), rat anti-mCherry (ThermoFisher; 1:2000), rabbit anti-Fos (Synaptic Systems; 1:1000), rabbit anti-Esr1 (Millipore; 1:10000), and rabbit anti-TH (Aves; 1:500). Secondary antisera were Alex Fluor 488 donkey anti-sheep (Jackson ImmunoResearch; 1:300), Alexa Fluor 488 donkey anti-rabbit (Jackson ImmunoResearch; 1:300), Cy3 donkey anti-rat (Jackson ImmunoResearch; 1:800), Cy3 donkey anti-rabbit (Jackson ImmunoResearch; 1:800), Cy5 donkey anti-chicken (Jackson ImmunoResearch; 1:500), and Alexa Fluor 647 donkey anti-rabbit (Jackson ImmunoResearch; 1:500). Optic fiber and GRIN lens placement above target locations was verified for all mice, and Fos induction by ChR2 was confirmed by immunostaining for Fos in mice perfused 1 hr after 5 min of laser illumination. To determine the co-expression of *Tac1* and Rabies-EGFP, we performed fluorescent hybridization chain reaction based *in situ* hybridization for *Tac1* in combination with the natural fluorescence emitted by Rabies-EGFP. We recently described this HCR ISH protocol in detail[9]. The *Tac1* HCR ISH probes and fluorescent amplifiers conjugated to AlexaFluor-647 were purchased from Molecular Instruments (Pasadena, CA). Sections were imaged using confocal microscopy (LSM800, Zeiss) and quantified using ImageJ software (NIH) as described previously[9,10,12].

Drugs—Females used as stimulus animals in mating assays were hormonally primed as described before[10]. In brief, females were injected subcutaneously with 10 μg of 17-β-estradiol benzoate (Sigma, cat# E8515) in 100 μL sesame oil at 48 hours before the assay, 5 μg in 50 μL sesame oil at 24 hours before the assay, and 50 μg of progesterone (Sigma, cat# P0130) in 50 μL sesame oil at 4–6 hours before the assay on the day of the mating test.

CNO solution was prepared as previously described[10]. In brief, CNO (Enzo) was dissolved in sterile saline at 5 mg/mL, aliquots were frozen, and each aliquot was freshly diluted with sterile saline prior to intra-peritoneal (i.p.) administration. The final dose of CNO for chemogenetic studies was 1 mg/kg.

Substance P (Sigma, Cat# S6883) was dissolved in sterile saline. For local infusion into POA, 200 nL of Substance P (10 ng) was infused per side, a dose based on a previous study[55]. For slice recording, Substance P was dissolved in ddH_2O to a stock concentration of 1 mM and diluted in ACSF to 50 nM for bath application. This concentration was chosen because it is ~2-fold > its EC_{50} (28 nM)[58].

L-703,606, (Sigma, # L119) was chosen as the Tacr1 antagonist for use in our studies as i.p. injection of 10 mg/kg of L-703,606 into male mice has previously been shown to disrupt recognition of female urine[56]. Therefore, we used the same 10 mg/kg dose for our Tacr1

antagonist studies with i.p. injections. As in published studies, L-703,606 was dissolved in 45% 2-hydroxypropyl-β-cyclodextrin to a stock concentration of 10 mg/mL (Sigma, cat# 332607). For local infusion into the POA, 1 μL of L-703,606 (500 pmol) was infused per side. This dose was chosen based on published doses of similar Tacr1 antagonists infused into other brain regions[114,115]. For slice recording, L-703,606 was dissolved in dimethyl sulfoxide (DMSO, Sigma) to a stock concentration of 10 mM and diluted to 10 μM in ACSF during recording.

Picrotoxin (PTX), was dissolved in DMSO to a stock concentration of 100 mM and diluted to 100 μM during recording.

6OHDA was used to ablate TH^+ neurons in the AVPV/PVpo as previously described[116]. On the day of the injection, the buffer solution was made, and 6OHDA (Sigma #H4381) was dissolved to 10 mg/ml in 0.1% ascorbic acid saline (0.9 % NaCl and 0.1 % Ascorbic acid; Sigma # PHR1008) and filter-sterilized. Bilateral stereotaxic injection of 1 μL of 6OHDA solution was delivered to empirically determined coordinates for the AVPV/PVpo (+/− 0.30 mm ML, +0.25 mm AP, and −5.50 mm DV).

The sodium channel blocker, tetrodotoxin (TTX), was used to inhibit POA activity during optogenetic activation of POA^{Tacr1} projections. TTX was diluted to a concentration of 1 μM in sterile saline and bilaterally infused (0.4 μL/side) via cannula into the POA.

Fiber photometry—Fiber photometry was conducted as described previously[10,113]. Briefly, the implanted optic fiber cannula on the mouse was connected via a patch cable (RWD Life Science) to a previously described custom-built fiber photometry setup (Bayless et al., 2019). An excitation light emitted from a 473 nm diode laser (Omicron LuxX) passed through an optic chopper (Thorlabs, MC2000) running at 400 Hz, neutral density filters (Thorlabs NE10B-A, NE30B-A, NE50B-A), a GFP excitation filter (Thorlabs, MF369–35), a dichroic mirror (Semrock, FF495-Di03–25×36), and a fiber collimator (Thorlabs, F240FC) before being directed to the patch cable connected to the experimental mouse. Fluorescence emitted by GCaMP6s during the behavioral assay was then passed through a fiber collimator, a GFP emission filter (Thorlabs, MF525–39), and a dichroic mirror, and focused by a plano-convex lens (Thorlabs, LA1255-A) onto a femtowatt photoreceiver (Newport, 2151). The signal from the photoreceiver was relayed to a lock-in amplifier (Stanford Research System, SR810), which also received a phase lock-in signal from the optic chopper. The output signal from the amplifier was recorded on a computer via a data acquisition device (LabJack, U6-Pro) at a 250 Hz sampling rate.

Prior to any behavioral testing, mice were habituated to the weight and feel of the optic fiber cable. The cable was attached to the optic fiber implants on the mice, and mice were allowed to move freely in their home cages during 3 separate 15 min habituation sessions. Behavioral video files and fluorescence data were time-locked via a light flash present in both datasets that was initiated by a pulse generator (Doric OTPG-4). The raw fluorescence data was normalized to the median fluorescence of the 5 min baseline period before the entrance of any animal or object into the cage. For PETP, time zero was set to the start of a behavior or event of interest, and the average fluorescence during the time window 10 s prior to a

behavioral event was used as the normalization factor to calculate change in fluorescence from baseline (ΔF/F). For peri-event analysis of amplitude changes, the 95 percent peak fluorescence (peak ΔF/F) was calculated and compared for the 10 s time window before and after a behavioral event.

Miniscope calcium imaging—We used a miniaturized fluorescence microscopy setup (nVista, Inscopix) to perform miniscope calcium imaging. During imaging sessions, the baseplate cover was removed and a miniscope was mounted and secured with a side screw. To synchronize fluorescence signals with annotated behaviors, we aligned both the imaging data and behavior videos to the event of a LED flash captured by the camera and recorded in the imaging data by a LED-triggered TTL signal generated by a data acquisition device. We used identical LED power, lens focus, digital gain, exposure time, and recording frame rate for all sessions for the same animal.

Imaging data were loaded on Inscopix data processing software (IDPS, Inscopix) and the size of the image was cropped to the area of the GRIN lens. The cropped data was processed to rectify defective pixels, spatially down-sampled by a factor of two to reduce data size, filtered with a spatial bandpass to remove low and high spatial frequency content, and corrected for motion so that each pixel corresponded to the same location across all frames. Imaging data were then converted into ΔF/F values. To identify the spatial locations of neurons {spatial masks of identified regions of interest (ROIs)} and its associated fluorescence signal from the processed imaging data, a constrained nonnegative matrix factorization-extended (CNMF-E) algorithm was applied in IDPS[117]. Identified ROIs were further screened based on all pixels being singly connected, morphology, location in imaging field, size, dynamics of associated raw calcium signal, and signal:noise of calcium signal. Calcium signals associated with each identified ROI (neuron) were synchronized with annotated behaviors and z-scored based on the mean and standard deviation of the entire imaging session. To determine whether an identified ROI generated a significant response during a behavioral event, the mean z-score between −10 s and 0 s to the onset of the behavioral event was compared with that between 0 s and 10 s following the onset of the behavioral event. A ROI (neuron) was considered significantly activated if the mean z-score following the behavioral event (0–10s) was >2 σ above the mean z-score prior to the behavioral event (−10–0s).

Optogenetic manipulations—Optogenetic manipulations were conducted as described previously[10]. Briefly, the implanted optic fiber cannula on the mouse was connected via a patch cable (RWD Life Science) to a diode laser (Opto Engine). All optogenetic stimuli were produced by a pulse generator (Doric OTPG-4) that triggered a blue light (473 nm) laser for ChR2 and PPO studies and a yellow light (593.5 nm) laser for eNpHR3.0 studies. Laser illumination commenced as soon as an intruder was placed into the resident's cage. Descriptions of the laser parameters are detailed below for each experiment. As with fiber photometry, prior to any behavioral testing, mice were habituated to the weight and feel of the optic fiber cable. Mice were given 3 separate 15 min habituation sessions. Mice were tested on each behavioral assay once each with laser illumination and no laser illumination, with the order of "Laser on" and "Laser off" assays counterbalanced across mice.

Chemogenetic inhibition—Chemogenetic inhibition studies were performed as described previously[10]. Briefly, experimental mice were i.p. injected with CNO at 1 mg/kg or sterile saline 30 min prior to behavioral assays. Mice were tested on each behavioral assay once each with CNO and saline, with the order of CNO and saline administration counterbalanced across animals.

Tacr1 antagonist manipulations—Fifteen minutes prior to behavioral testing, the bilateral cannula (RWD Life Science) implanted above the POA of experimental males was connected to two Hamilton syringes via polyethylene tubing, loaded with 1 μL of L-703,606 (500 pmol) or control vehicle per side and infused slowly over a period of 2 min using a syringe pump (Harvard Apparatus). Needles were left connected for an additional 2 min and then withdrawn. Prior to any behavioral testing, mice were habituated to the handling and the weight and feel of being connected to the Hamilton syringes via polyethylene tubing. Mice were given 3 separate “mock infusion” habituation sessions on separate days.

Electrophysiology

Slice preparation: Brain slices (300 μm) were obtained using standard techniques. Briefly, animals were anesthetized with isoflurane and decapitated. The brain was exposed and chilled with ice-cold artificial cerebrospinal fluid (ACSF) containing 125 mM NaCl, 2.5 mM KCl, 2 mM $CaCl_2$, 1.25 mM NaH_2PO_4, 1 mM $MgCl_2$, 25 mM $NaHCO_3$, and 15 mM D-glucose. ACSF was saturated with 95% O_2 and 5% CO_2. Osmolarity was adjusted to 300–305 mOsm. Coronal brain slices containing BNST or POA were prepared with a vibrating microtome (Leica VT1200 S, Germany) and left to recover in ACSF for 30 min at 34°C and then at room temperature for an additional 30 min. Slices were then moved to a submerged recording chamber perfused with ACSF at a rate of 2–3 ml/min at 30–31°C, and brain slices were recorded within 5 hours after recovery.

Whole-cell recordings: To identify POA^{Tacr1} neurons, we injected AAV-DIO-tdTomato into the POA of $Tacr1^{Cre}$ males and prepared brain slices 4 weeks after viral delivery. POA neurons were visualized under infrared illumination using an Olympus BX51WI microscope equipped with Differential Interference Contrast (DIC), a water-immersion objective (40× NA 0.8), and a CMOS camera (Hamamatsu Photonics). TdTomato+ neurons were identified using fluorescence illumination (Lambda XL, Sutter instrument) coupled with a Texas Red filter set (Chroma Technology Corp).

To record spontaneous activity, whole-cell current-clamp with zero holding current (Ih = 0) was performed with borosilicate glass microelectrode (3–3.5 MΩ) filled with a K^+-based internal solution (135 mM $KMeSO_3$, 8.1 mM KCl, 10 mM HEPES, 8 mM Na^2-Phosphocreatine, 0.3 mM GTP-Na, 4 mM ATP-Mg, 0.1 mM $CaCl_2$, 1 mM EGTA; pH 7.2–7.3; osmolarity 285–290 mOsm). Baseline firing rate was recorded for at least 5 min, before Substance P perfusion or BNSTpr terminal stimulation. Substance P (1 μM) was applied in bath perfusion for 5 min while the membrane potential was continuously recorded for 10 min. To stimulate BNSTpr terminals, we injected AAV-ChR2:EYFP to the BNSTpr as well as AAV-DIO-tdTomato to the POA of $Tacr1^{Cre}$ males, and slices were prepared 8–10 weeks after viral delivery. BNSTpr terminals were stimulated with 90 s 473 nm

laser (OptoEngine) illumination (0.5 ms pulse, 5 Hz, 90 s) through the objective while the membrane potential responses of POA^{Tacr1} neurons were continuously recorded. To record optically evoked action potentials in ChR2+ BNSTpr neurons, whole-cell current-clamp (Ih = 0) was performed, and the same laser illumination as above was delivered.

To record AMPA/NMDA ratios and paired-pulse ratios, picrotoxin (100 μM) was included in the ACSF perfusion and whole-cell voltage-clamp was performed with a Cs^+-based internal solution (126 mM $CsMeSO_3$, 8 mM NaCl, 10 mM HEPES, 2.9 mM QX-314, 8 mM Na^2-Phosphocreatine, 0.3 mM GTP-Na, 4 mM ATP-Mg, 0.1 mM $CaCl_2$, 1 mM EGTA; pH 7.2–7.3; osmolarity 285–290 mOsm). Membrane potential was held at −70 mV to record AMPA receptor mediated current or +40 mV to record NMDA receptor-mediated current. Glutamatergic terminals were stimulated locally with a concentric bipolar microelectrode (FHC) placed 100–200 μm from the recorded POA^{Tacr1} neuron. Stimulation intensity (0.2 ms, 100–200 μA) was adjusted to evoke EPSCs with an amplitude of around 50–100 pA while recording at +40 mV. AMPA/NMDA ratios were calculated by dividing the amplitude of AMPA current, measured as the peak current at −70 mV, by the amplitude of NMDA current, measured at 50 ms after stimulus at +40 mV when the contribution of the AMPA component was minimal. In the same neurons, two EPSCs were evoked 50 ms apart while being recorded at −70 mV, and the paired-pulse ratio was calculated by dividing the peak amplitude of the second EPSC by the first.

Recordings were obtained with a Multiclamp 700B amplifier (Molecular Devices) using the WinWCP software (University of Strathclyde, UK). Liquid junction potential was not corrected. Signals were filtered at 2 kHz, digitized at 10 kHz (NI PCIe-6259, National Instruments), and analyzed offline using Matlab (Mathworks).

Perforated patch and LTP recording: Electrical access to the POA^{Tacr1} neurons was achieved through the perforated-patch method using Gramicidin A (Sigma). Perforated patch was performed with a borosilicate glass microelectrode (3–3.5 MΩ), front-filled with 1 μl K^+-based internal solution and back-filled with 10 μl Gramicidin A-containing internal solution. The Gramicidin A-containing internal solution was made fresh before use: Gramicidin A (Sigma) was dissolved in DMSO to 20 mg/mL and then diluted in the K^+-based internal solution yielding a final concentration of 200 μg/mL. The solution was thoroughly mixed by vortexing and then sonicated for 5 min and filtered with a centrifuge tube filter (0.22 μm, Spin-X, Costar). After the microelectrode formed a giga seal with the cell membrane, access resistance was continuously monitored during perforation by applying a −5 mV pulse from a holding potential of −70 mV, under the voltage-clamp mode. A stable perforated patch normally formed within 30–60 minutes, and the access resistance stayed around 30–50 MΩ without further decreasing. Then the recording was switched to current-clamp mode. The membrane potential was adjusted to ~−70 mV by injecting a negative holding current (Ih = − 50–200 pA) since POA^{Tacr1} neurons were intrinsically firing. The serial resistance was compensated with amplifier bridge balance. The data were excluded if the input resistance (R_{in}) changed more than 25% over the course of the experiment.

Picrotoxin (100 μM) was included in ACSF perfusion throughout the recording, EPSPs were evoked by focal extracellular stimulation at 0.05Hz with a small theta glass electrode positioned 50–100 μm from the recorded cell body. Stimulation intensity (0.2 ms, 5–30 μA) was adjusted to evoke stable EPSPs with an amplitude of around 2–5 mV. Basal EPSPs were recorded for at least 5 min, before LTP was induced by Substance P perfusion or BNSTpr terminal stimulation. Substance P (50 nM) was applied in bath perfusion for 5 min, and EPSPs were continuously recorded for another 25 min to monitor the change of amplitudes. BNSTpr terminals were stimulated with 90 s 473 nm laser illumination as above, and EPSPs were recorded afterwards for 30 min. For Tacr1 antagonist experiments, L-703,606 (10 μM) was added in ACSF perfusion throughout the recordings.

Behavioral testing—All behavioral testing was initiated ≥ 1 hr after onset of the dark cycle and recorded using camcorders (Sony) under infrared illumination as described previously[10]. Videos were played at 30 frames per second and manually annotated using custom software described previously[11,118,119]. This permitted analysis of multiple parameters (including number, duration, latency, probability, and inter-event interval) of different behavioral routines. In particular, anogenital investigation (sniff), mounting, repeated pelvic thrust (intromission), and ejaculation were scored for sexual behaviors. Aggression was scored as occurring when physical attacks (episodes of biting, wrestling, tumbling, chasing) were observed.

Both sexual and aggressive displays were annotated during female-male and male-male interactions. Male-female interactions lasted for 30 min to enable display of different mating routines. Male-male interactions were restricted to 15 min to allow fighting to occur but were short enough to preclude excessive attacks toward intruders. When female and male mating were directly compared, the behavioral statistics for interactions with female intruders were derived from only including behaviors that occurred in the first 15 min of the assay to make the analysis window the same as the 15 min assay with the male intruder. All behavioral studies were conducted using previously published procedures[11,20,118–120]. The various behavioral assays used in the study are described briefly below.

Behaviors for Fig. 1, S1: To examine the response of sexually naïve male BNSTpr^{Tac1} neurons to pheromones (Fig. 1B-E), sexually naïve males with GCaMP6s expressed in and optic fibers above BNSTpr^{Tac1} neurons were single housed for ≥ 7 days prior to fiber photometry studies. Males were exposed for 3 min on separate days in their home cage to a 1”x1” cotton swab wetted with 80 μl of undiluted urine from urine from WT group housed primed C57BL/6J females, WT group housed C57BL/6J males, or saline. The order of the swab assays was counterbalanced across mice. Urine was collected 3–6 hours prior to use and kept on ice until pipetted onto the swab.

To examine the response of sexually naïve male BNSTpr^{Tac1} neurons during initial encounters with females and males (Fig. S1A-E), after completion of urine swab assays, males were exposed for 3 min on separate days in their home cage to a WT group housed hormonally primed female, a WT group housed male, or an inanimate toy mouse, with the order of the intruder assays counterbalanced across mice. The short 3 min assays precluded the occurrence of any mating or aggression displays during the assays.

To examine the response of male BNSTpr^{Tac1} neurons during mating and aggression (Fig. S1F-M), after completion of the brief encounter assays, males were assayed on separate days in their home cage during a 30 min interaction with a WT group housed hormonally primed female and a 15 min interaction with a WT group housed male. For both assays, males had no prior experience mating with a female intruder or attacking a male intruder. We imaged GCaMP6s fluorescence in multiple assays until the experimental male exhibited typical social displays, mating toward female intruder and aggression toward male intruder. Most males showed social behaviors even in the first assay (3/6 mated with females and 4/6 attacked males), and all males exhibited mating with females and aggression with males within 3 rounds of testing. In our imaging studies using sexually naïve males, we did not observe any significant increase in the Ca^{2+} activity of BNSTpr^{Tac1} neurons during attack bouts. However, in a recent study[121], we did observe an increase in Ca^{2+} activity of BNSTpr^{Tac1} neurons during attack bouts of males that had extensive mating and aggression experience. Together, these findings indicate that mating and/or aggression experience increases the responsivity of BNSTpr^{Tac1} neurons during attack bouts.

To examine the response of individual BNSTpr^{Tac1} neurons to pheromones (Fig. 1F-N, S1N-O), sexually naïve males with GCaMP6s expressed in and GRIN lenses above BNSTpr^{Tac1} neurons were single housed for ≥ 7 days prior to miniscope imaging studies. Males were exposed for 3 min each in their home cage to a 1”x1” cotton swab wetted with 80 μl of undiluted urine from WT group housed primed C57BL/6J females, WT group housed C57BL/6J males, or saline. To ensure reliable imaging from the same set of BNSTpr^{Tac1} neurons in response to each swab, the swabs were presented during the same imaging session with the order of the presentation of the swabs counterbalanced across mice and a 7 min interval between swab presentations. Urine was collected 3–6 hours prior to use and kept on ice until pipetted onto the swab.

To examine the effect of optogenetic activation of BNSTpr^{Tac1} neurons during social interactions with males and females (Fig. 1O-V, S1P-V), sexually naïve males with ChR2 expressed in and optic fibers above BNSTpr^{Tac1} neurons were single housed for ≥ 7 days prior to behavioral testing. To assay male-female interactions, a WT group-housed hormonally primed female was inserted into the experimental male’s home cage for 30 min. To assay male-male interactions, a WT group-housed male was inserted into the experimental male’s home cage for 15 min. Laser illumination parameters were based on published parameters for BNSTpr^{Aro} neurons that promote male-male mating[10]. For transient photostimulation, laser illumination (473 nm, 5 Hz, 5 ms pulse width, 8 mW from the fiber tip) was provided for the first 90s of the assay, and then illumination was turned off for the rest of the assay. For intermittent photostimulation, laser illumination (473 nm, 5 Hz, 5 ms pulse width, 8 mW from the fiber tip) was provided in cycles of 30 s laser on and 30 s laser off throughout the entire assay.

Behaviors for Fig. 2, S2: To examine the effect of optogenetic activation of BNSTpr^{Tac1}→POA projections during social interactions with males and females (Fig. 2J-L, S2A-H), sexually naïve males with ChR2 expressed in BNSTpr^{Tac1} neurons and optic fibers above the POA were single housed for ≥ 7 days prior to behavioral testing. Behavioral assays and transient photostimulation were performed as described above for Fig. 1O-V.

To examine the effect of optogenetic inhibition of BNSTpr^{Tac1}→POA projections during social interactions with males and females (Fig. 2M-Q, S2I-R), sexually naïve males with PPO expressed in BNSTpr^{Tac1} neurons and optic fibers above the POA were single housed for ≥ 7 days prior to behavioral testing. Behavioral assays were performed as described above for Fig. 1O-V. Laser illumination parameters were based on published parameters that inhibit synaptic transmission at axon terminals[48]. Laser illumination (473 nm, 10 Hz, 10 ms pulse width, 8 mW from the fiber tip) was delivered constantly for the entire assay.

Behaviors for Fig. 3, S3: To examine the response of male POA^{Tacr1} neurons during mating and aggression (Fig. 3A-F, S3E-I), sexually naïve males with GCaMP6s expressed in and optic fibers above POA^{Tacr1} neurons were single housed for ≥ 7 days prior to fiber photometry studies. Behavioral assays were performed as described above for Fig. S1F-M.

To examine the effect of optogenetic activation of POA^{Tacr1} neurons during social interactions with males and females (Fig. 3G-N, S3J-N), sexually naïve males with ChR2 expressed in and optic fibers above POA^{Tacr1} neurons were single housed for ≥ 7 days prior to behavioral testing. Behavioral assays were performed as described above for Fig. 1O-V. Laser illumination parameters were based on published parameters for POA^{Esr1} neurons that elicit mating behavior[17]. Laser illumination (473 nm, 40 Hz, 10 ms pulse width, 8 mW from the fiber tip) was provided in cycles of 15 s laser on and 45 s laser off throughout the entire assay.

To examine the effect of optogenetic activation of POA^{Tacr1} neurons during interactions with inanimate objects (Fig. 3O-V), after completion of social interaction assays, males were given separate 2 min interaction assays with a range of inanimate object and mouse stimuli. During each assay, laser illumination (473 nm, 40 Hz, 10 ms pulse width, 8 mW from the fiber tip) was provided for two cycles of 30 s laser off and 30 s laser on. The order of the object interaction assays was counterbalanced across mice.

To examine the effect of optogenetic activation of POA^{Tacr1} neurons on USV production (Fig. 3N-Q), sexually naïve group housed males were tested in a clean cage alone with no social stimulus. An ultrasonic microphone (Noldus, Pettersson M500–384 ultrasonic microphone) was placed above the testing cage. During the assay, laser illumination (473 nm, 40 Hz, 10 ms pulse width, 8 mW from the fiber tip) was provided for three cycles of 30 s laser off and 30 s laser on. The USV frequency analysis window was restricted to 50k Hz – 80,000k Hz and analyzed using Noldus UltraVox XT software.

Behaviors for Fig. 4, S4: To examine the effect of optogenetic inhibition of POA^{Tacr1} neurons during social interactions with males and females (Fig. 4A-K, S3R-U), sexually naïve males with eNpHR3.0 expressed in and optic fibers above POA^{Tacr1} neurons were single housed for ≥ 7 days prior to behavioral testing. Behavioral assays were performed as described above for Fig. 1O-V. Laser illumination parameters were based on published parameters for BNSTpr^{Aro} neurons that inhibit male mating behaviors[10]. For constant inhibition studies, laser illumination (593.5 nm, 6 mW from the fiber tip) was on throughout the entire assay. For mount-triggered inhibition studies, laser illumination (593.5 nm, 6 mW from the fiber tip) was delivered immediately upon mounting of a female. Laser illumination

was turned off as soon as the mounting behavior ended. This paradigm was repeated for each subsequent mounting attempt.

To examine the effect of optogenetic activation of BNSTpr^{Esr1} neurons in combination with chemogenetic inhibition of POA^{Tacr1} neurons during social interactions with males and females (Fig. 4L-P, S4A-P), sexually naïve males with ChR2 expressed in and optic fibers above BNSTpr^{Esr1} neurons and DREADDi expressed in POA^{Tacr1} neurons were single housed for ≥ 7 days prior to behavioral testing. Behavioral assays and laser illumination parameters were performed as described above for Fig. 1O-V. CNO at 1 mg/kg or control saline was i.p. injected into males 30 min prior to behavioral assays with the order of the CNO and control injection assays counterbalanced across mice.

To examine the effect of chemogenetic inhibition of POA^{Tacr1} neurons on non-social behaviors, experimental males were also assayed for performance in locomotor activity (Fig. S4J), latency to find hidden food (Fig. S4K), and elevated plus maze (Fig. S4L), as described previously[11,20,119]. Briefly, males were tested for locomotor activity by quantifying the number of midline crosses that each male made during a social interaction. Then, males were tested for olfactory motivated behavior with a food finding assay. After being food deprived for 6hrs, males were inserted into a clean cage with a cracker (Cheez-It) buried under the bedding. Males were given 5 min to find the cracker at which time the assay ended. Latency to find the food was scored. Then, males were tested for anxiety-like behavior with the elevated plus maze. Males were placed in the center of an elevated plus maze facing the open arm at the start of the assay. Time spent in the closed or open arms during the 5 min assay was scored. Mice were given ≥1 days between each behavioral test. Chemogenetic inhibition was performed as described above for Fig. 4L-P.

To examine the effect of optogenetic activation of POA^{Tacr1} neurons in combination with chemogenetic inhibition of BNSTpr^{Esr1} neurons during social interactions with males and females (Fig. 4Q-U, S4Q-Y), sexually naïve males with ChR2 expressed in and optic fibers above POA^{Tacr1} neurons and DREADDi expressed in BNSTpr^{Esr1} neurons were single housed for ≥ 7 days prior to behavioral testing. Behavioral assays were performed as described above for Fig. 1O-V. Laser illumination parameters were performed as described above for Fig. 3G-N. Chemogenetic inhibition was performed as described above for Fig. 4L-P.

To test for effects of laser illumination absent expression of optogenetic actuators, we expressed mCherry in male POA^{Tacr1} neurons instead of ChR2 (Fig. 3G-V, S3J-M) or eNpHR3.0 (Fig. 4A-K, S3R-U). We assayed these control mice using the behavioral tests and laser illumination paradigms described for experimental mice expressing ChR2 or eNpHR3.0. The same cohort of control mice was tested without light or with 473 nm or 593.5 nm laser illumination. Pairwise comparisons between no-light and laser illumination conditions revealed no effect of light and are reported in Table S3.

Behaviors for Fig. 5, S5, S6: To examine the effect of encountering a female on the AMPA/NMDA ratio and paired-pulse ratio of POA^{Tacr1} neurons (Fig. 5I-M, S5L-O), sexually naïve males were single-housed for ≥ 7 days prior to behavioral testing. L-703,606 at 10 mg/kg or

control vehicle was injected i.p. into experimental males. After 30 min, the male continued to be singly-housed for 15 min or a hormonally primed sexually receptive WT female was inserted into the male's cage for 15 min. No mounting of the female was observed in these 15 min for assays in which the male was used for electrophysiology studies shown in this study. At the end of behavioral assays, male mice were anesthetized and brains were collected for slice preparation and recording.

To examine the effect of local POA infusion of Substance P during social interactions with females (Fig. 5N-P, S6B-C), sexually naïve males with bilateral cannulas placed above the POA were single-housed for ≥ 7 days prior to behavioral testing. Behavioral assays were performed as described above (Fig. 1O-V). Fifteen min prior to behavioral assays, 200 nL of Substance P (10 ng) or control vehicle was infused per side into the POA. The order of Substance P and vehicle infusion was counterbalanced across mice and performed ≥2 days apart.

To examine the effect of local POA infusion of the Tacr1 antagonist, L-703,606, during social interactions with males and females (Fig. 5Q-S, S6D-J), sexually naïve males with bilateral cannulas placed above the POA were single housed for ≥ 7 days prior to behavioral testing. Behavioral assays were performed as described above for Fig. 1O-V. Fifteen min prior to behavioral assays, 1 μL of L-703,606 (500 pmol) or control vehicle was infused per side into the POA. The order of L-703,606 and control infusion assays were counterbalanced across mice and performed ≥2 days apart.

To examine the effect of optogenetic activation of BNSTpr^{Tac1}→POA projections in combination with systemic administration of the Tacr1 antagonist, L-703,606, during social interactions with males and females (Fig. 5T-X, S6K-N), following experiments of Fig. 2J-L, S2A-H, males with ChR2 expressed in BNSTpr^{Tac1} neurons and optic fibers above the POA were used for behavioral testing. Behavioral assays and laser illumination parameters were performed as described above for Fig. 1O-V. L-703,606 at 10 mg/kg or control vehicle was i.p. injected into males 30 min prior to behavioral assays with the order of the L-703,606 and control injection assays counterbalanced across mice.

To examine the effect of optogenetic activation of POA^{Tacr1} neurons in combination with systemic administration of the Tacr1 antagonist, L-703,606, during social interactions with males and females (Fig. S6O-U), following experiments of Fig. 3G-N, S3J-M, males with ChR2 expressed in and optic fibers above POA^{Tacr1} neurons were used for behavioral testing. Behavioral assays and laser illumination parameters were performed as described above for Fig. 3G-N. L-703,606 administration was performed as described above for Fig. 5T-X.

Behaviors for Fig. 6, S7: To examine the effect of optogenetic activation of POA^{Tacr1} neurons during the post-ejaculatory refractory period (Fig. 6A-D, S7A-C), males with ChR2 expressed in and optic fibers above POA^{Tacr1} neurons were single housed for ≥ 7 days prior to behavioral testing. Prior to measuring refractory period behavior, the experimental males were allowed to interact with a female until ejaculation. In a subset of the mating assays, POA^{Tacr1} neurons were activated to ensure that mating behavior and ejaculation occurred.

Refractory period mating experiments began when the male became ambulatory after the initial ejaculation. The refractory period mating assay consisted of a 30 min assay with a WT female intruder. Laser illumination (473 nm, 40 Hz, 10 ms pulse width, 5 mW from the fiber tip) was provided in cycles of 30 s laser on and 30 s laser off throughout the entire refractory period mating assay. Laser illumination and no laser illumination assays were counterbalanced and performed at least one week apart. In a subset of the assays, the female that received the initial ejaculation was replaced by a new WT female. In these cases, the male interacted with a new female during both the laser illumination and no laser illumination assays.

To examine the effect of optogenetic activation of POA^{Tacr1} neurons during the real time social place preference assay (Fig. 6E-I, S7D-E), males with ChR2 expressed in and optic fibers above POA^{Tacr1} neurons were single housed for ≥ 7 days prior to behavioral testing. In the real time social place preference assay, experimental males were permitted to freely explore a rectangular (19.5 cm x 13.0 cm) behavioral arena. At the ends of the arena were two containers, one which was empty and the other which contained a stimulus WT female. The containers were constructed by securing together two disposable feeders (Innovive), and both experimental and stimulus animals were acclimated to the behavior arena for 10 minutes 1 day prior to the experiment. Each experimental mouse underwent three 10 minute trials: “Laser off” in which there was no laser illumination, “Laser on, female side” in which laser illumination (473 nm, 40 Hz, 10 ms pulse width, 5 mW from the fiber tip) was provided only when the experimental mouse was located in the half of the behavior arena containing the stimulus female, and “Laser on, empty side” in which laser illumination (same as above) was provided only when the experimental mouse was located in the half of the behavior arena with the empty container. The location of the experimental mouse was tracked using custom code (MATLAB). The 3 trials were conducted consecutively, with the “Laser off” trial always occurring first and the “Laser on, female side” and “Laser on, empty side” being counterbalanced across mice. Female preference index was calculated as (investigate female container – investigate empty container) / (investigate female container + investigate empty container). Sniffing or placement of forepaws onto the female or empty container was manually classified as investigation behavior, and duration of investigation behavior towards the containers was quantified to construct the female preference index.

To test if males perform self-stimulation for optogenetic activation of POA^{Tacr1} neurons (Fig. 6J-L, S7F-G), males with ChR2 expressed in and optic fibers above POA^{Tacr1} neurons were single housed for ≥ 7 days prior to behavioral testing. In the optogenetic self-stimulation assay, experimental males were permitted to freely explore a behavior chamber containing two ports. Each mouse was acclimated to the behavior chamber for 10 minutes 1 day prior to the experiment. When the mouse made a nose poke to the port designated as “active,” the mouse received a short period of laser illumination (0.5 s, 473 nm, 40 Hz, 10 ms pulse width, 5 mW from the fiber tip). When the mouse made a nose poke to the other port, designated “inactive”, nothing happened. Each experimental mouse underwent two 10 min trials with the identity of the “active” port alternating between the two port locations in each trial. The two trials were performed consecutively, and the order of the active ports were counterbalanced. Each trial began when the mouse made a nose poke to both ports at least once. For the experiments of Fig. 6J-L, S7F-G, initiation of

laser illumination and nose-poke quantification were performed manually from an overhead camera. For the experiments of Fig. 7F,H,I,M,N, S9E-F) custom code and Arduino were used for initiation of laser illumination and nose-poke quantification.

To examine the effect of optogenetic inhibition of POA^{Tacr1} neurons during the real time social place preference assay (Fig. 6M-N), males with eNPHR3.0 expressed in and optic fibers above POA^{Tacr1} neurons were single housed for ≥ 7 days prior to behavioral testing. The real time social place preference assay was performed as described above for Fig. 6E-I. “Laser off”, “Laser on, female side”, and “Laser on, empty side” trials were performed as described above for Fig. 6E-I, except with 593.5 nm laser illumination constant at 5 mW from the fiber tip.

To examine the effect of optogenetic inhibition of POA^{Tacr1} neurons during sucrose consumption (Fig. 6O-P), males with eNPHR3.0 expressed in and optic fibers above POA^{Tacr1} neurons were tested on a sucrose consumption assay. In the sucrose consumption assay, an experimental mouse was permitted to freely explore a rectangular behavior arena (19.0 cm x 28.5 cm) containing a spout on one end of the arena that dispensed water or sucrose water. When the mouse drank from the spout, the spout dispensed additional liquid once the mouse crossed the midpoint of the arena. A repeating pipette was manually used to dispense 4 uL liquid. Mice were acclimated to the arena 1 day before the first trial and gained experience drinking from a spout that dispensed 30% sucrose water. In a 10 min trial, the number of times the mouse drank the liquid and crossed the midpoint of the arena was quantified. During “Laser on” trials, the mouse received constant 5 mW 593.5 nm laser illumination, and during “Laser off” trials, no laser illumination was provided. The trials were conducted in a block of two consecutive trials of “Laser on” and “Laser off” for each concentration of sucrose (0%, 15%, and 30%), and each block was performed twice, with one block performing the “Laser on” trial first and the other block performing the “Laser off” trial first. Each block was performed at least two days apart.

Behaviors for Fig. 7, S8, S9: To examine the effect of optogenetic activation of POA^{Tacr1} neurons during the post-ejaculatory refractory period in males with ablated $AVPV/PVpo^{TH}$ neurons (Fig. 7A-D, S8A-D), males with ChR2 expressed in and optic fibers above POA^{Tacr1} neurons and injected with 6OHDA or control vehicle into the AVPV/PVpo were single housed for ≥ 7 days prior to behavioral testing. Refractory period mating experiments and laser illumination conditions were performed as described above for Fig. 6A-D.

To examine the effect of optogenetic activation of POA^{Tacr1} neurons during the real time social place preference assay in males with ablated $AVPV/PVpo^{TH}$ neurons (Fig. 7E), males with ChR2 expressed in and optic fibers above POA^{Tacr1} neurons and injected with 6OHDA or control vehicle into the AVPV/PVpo were assayed. Real time social place preference experiments and laser illumination conditions were performed as described above for Fig. 6E-I.

To test if males with ablated $AVPV/PVpo^{TH}$ neurons perform self-stimulation for optogenetic activation of POA^{Tacr1} neurons (Fig. 7F), males with ChR2 expressed in and optic fibers above POA^{Tacr1} neurons and injected with 6OHDA or control vehicle into the

AVPV/PVpo were assayed. Optogenetic self-stimulation experiments and laser illumination conditions were performed as described above for Fig. 6J-L.

To test if males perform self-stimulation for optogenetic activation of POA^{Tacr1}→VTA projections (Fig. 7G-I), males with ChR2 expressed in POA^{Tacr1} neurons and optic fibers above the VTA were single housed for ≥ 7 days prior to behavioral testing. Optogenetic self-stimulation experiments and laser illumination conditions were performed as described above for Fig. 6J-L.

To examine the effect of optogenetic activation of POA^{Tacr1}→VTA projections during social interactions with males and females (Fig. 7J-K, S9A-B), males with ChR2 expressed in POA^{Tacr1} neurons and optic fibers above the VTA were assayed. Behavioral assays were performed as described above for Fig. 1O-V, and laser illumination conditions were performed as described above for Fig. 3G-N.

To test if males perform self-stimulation for optogenetic activation of POA^{Tacr1}→PAG projections (Fig. 7L-N), males with ChR2 expressed in POA^{Tacr1} neurons and optic fibers above the PAG were single housed for ≥ 7 days prior to behavioral testing. Optogenetic self-stimulation experiments and laser illumination conditions were performed as described above for Fig. 6J-L.

To examine the effect of optogenetic activation of POA^{Tacr1}→PAG projections during social interactions with males and females (Fig. 7O-P, S9C-D), males with ChR2 expressed in POA^{Tacr1} neurons and optic fibers above the PAG were assayed. Behavioral assays were performed as described above for Fig. 1O-V, and laser illumination conditions were performed as described above for Fig. 3G-N.

To examine if silencing of POA activity alters the behavioral effects of optogenetic activation of POA^{Tacr1}→VTA or PAG projections during the self-stimulation assay (Fig. S9E-F) or during social interactions with males and females (Fig. S9G-J), males with ChR2 expressed in and bilateral cannula placed above POA^{Tacr1} neurons and optic fibers above the VTA or PAG were assayed. For optogenetic self-stimulation experiments, behavioral assays and laser illumination conditions were performed as described above for Fig. 6J-L. For social interaction assays, behavioral assays were performed as described above for Fig. 1O-V, and laser illumination conditions were performed as described above for Fig. 3G-N. Twenty min prior to behavioral assays, 0.4 μL of 1 μM TTX or control vehicle was manually infused per side into the POA over a period of 2 min. The order of TTX and control infusion assays were counterbalanced across mice and performed ≥2 days apart.

To test if optogenetic activation of POA^{Tacr1}→VTA projections elicited DA release in NAc, ChR2 (Fig. 7Q-T) or control AAV (Fig. S9N-P) was expressed in POA^{Tacr1} neurons and $GRAB_{DA}$ was expressed constitutively in NAc. Optic cables were placed dorsal to the VTA and NAc for activation and imaging, respectively. Pilot experiments were attempted to place optic cables over the POA and the NAc, but the two regions' proximity to each other precluded this configuration. While recording $GRAB_{DA}$ signal from NAc, laser illumination (473 nm, 40 Hz, 10 ms pulse width, 5 mW from the fiber tip) was provided to the VTA for

10 seconds. For $GRAB_{DA}$ photometry during repeated activation of VTA (Fig. 7T), the same laser 10 s laser illumination was applied 6 times with 30 s intervals.

QUANTIFICATION AND STATISTICAL ANALYSIS

Calcium imaging data, behavioral video recordings, electrophysiological studies, and histological samples were conducted or analyzed blind to relevant variables, including identity of administered solutions, genotypes, light illumination conditions, surgical procedures, and viruses injected. Statistical analysis was performed using GraphPad PRISM (GraphPad Software). To compare categorical data including percentage of mice displaying a behavior, Fisher's exact test was performed from a 2×2 contingency table. To compare non-categorical data, we first determined if the data values were from a normal distribution using the D'Agostino-Pearson omnibus normality test. In experiments with paired samples, we used a paired t test or repeated measures ANOVA for parametric data and a Wilcoxon matched-pairs signed rank test or Friedman test for non-parametric data. In all other experiments, we used a t test or ANOVA for parametric data and a Mann-Whitney or Kruskal-Wallis test for non-parametric data. All multiple comparisons were corrected for using Bonferroni corrections.

Supplementary Material

Refer to Web version on PubMed Central for supplementary material.

ACKNOWLEDGMENTS

We thank Richard Axel, Tom Clandinin, Julie Kauer, and Shah lab members for feedback, Daniel Cardozo Pinto for sharing reagents, and Maricruz Alvarado and Lily Duong for research support and administration. This work was supported by grants to VMAC (Pew Charitable Trust Fellowship #00036063), JBD (GG Gift Fund), COD (NSF GRFP 2018265046 and PD Soros Fellowship for New Americans), LL (R01NS050835) NMS (NIH R01NS049488; R01HD104565), YW (SoM Dean's Fellowship), and RY (Wu Tsai interdisciplinary award, NIH F32HD113431).

INCLUSION AND DIVERSITY

One or more of the authors of this paper self-identifies as an underrepresented ethnic minority in their field of research or within their geographical location, or living with a disability, or has received support from a program designed to increase minority representation in their field of research. While citing references scientifically relevant for this work, we also actively worked to promote gender balance in our reference list.

REFERENCES

1. Triggs GS (1991). The population ecology of house mice (Mus domesticus) on the Isle of May, Scotland. Journal of Zoology 225, 449–468. 10.1111/j.1469-7998.1991.tb03828.x.
2. Bronson FH (1979). The reproductive ecology of the house mouse. Q Rev Biol 54, 265–299. [PubMed: 390600]
3. King JA (1956). Sexual behavior of C57BL/10 mice and its relation to early social experience. The Journal of Genetic Psychology 88, 223–229. [PubMed: 13406250]
4. Mandiyan VS, Coats JK, and Shah NM (2005). Deficits in sexual and aggressive behaviors in Cnga2 mutant mice. Nat. Neurosci. 8, 1660–1662. 10.1038/nn1589. [PubMed: 16261133]

5. Leypold BG, Yu CR, Leinders-Zufall T, Kim MM, Zufall F, and Axel R. (2002). Altered sexual and social behaviors in trp2 mutant mice. Proc. Natl. Acad. Sci. U.S.A. 99, 6376–6381. 10.1073/pnas.082127599. [PubMed: 11972034]
6. Stowers L, Holy TE, Meister M, Dulac C, and Koentges G. (2002). Loss of sex discrimination and male-male aggression in mice deficient for TRP2. Science 295, 1493–1500. 10.1126/science.1069259. [PubMed: 11823606]
7. Yoon H, Enquist LW, and Dulac C. (2005). Olfactory inputs to hypothalamic neurons controlling reproduction and fertility. Cell 123, 669–682. 10.1016/j.cell.2005.08.039. [PubMed: 16290037]
8. Wang Z, Sindreu CB, Li V, Nudelman A, Chan GC-K, and Storm DR (2006). Pheromone Detection in Male Mice Depends on Signaling through the Type 3 Adenylyl Cyclase in the Main Olfactory Epithelium. J. Neurosci. 26, 7375–7379. 10.1523/JNEUROSCI.1967-06.2006. [PubMed: 16837584]
9. Knoedler JR, Inoue S, Bayless DW, Yang T, Tantry A, Davis C, Leung NY, Parthasarathy S, Wang G, Alvarado M, et al. (2022). A functional cellular framework for sex and estrous cycle-dependent gene expression and behavior. Cell 185, 654–671.e22. 10.1016/j.cell.2021.12.031. [PubMed: 35065713]
10. Bayless DW, Yang T, Mason MM, Susanto AAT, Lobdell A, and Shah NM (2019). Limbic Neurons Shape Sex Recognition and Social Behavior in Sexually Naive Males. Cell 176, 1190–1205.e20. 10.1016/j.cell.2018.12.041. [PubMed: 30712868]
11. Yang CF, Chiang MC, Gray DC, Prabhakaran M, Alvarado M, Juntti SA, Unger EK, Wells JA, and Shah NM (2013). Sexually dimorphic neurons in the ventromedial hypothalamus govern mating in both sexes and aggression in males. Cell 153, 896–909. 10.1016/j.cell.2013.04.017. [PubMed: 23663785]
12. Yang T, Yang CF, Chizari MD, Maheswaranathan N, Burke KJ, Borius M, Inoue S, Chiang MC, Bender KJ, Ganguli S, et al. (2017). Social Control of Hypothalamus-Mediated Male Aggression. Neuron 95, 955–970.e4. 10.1016/j.neuron.2017.06.046. [PubMed: 28757304]
13. Lee H, Kim D-W, Remedios R, Anthony TE, Chang A, Madisen L, Zeng H, and Anderson DJ (2014). Scalable control of mounting and attack by Esr1 + neurons in the ventromedial hypothalamus. Nature 509, 627–632. 10.1038/nature13169. [PubMed: 24739975]
14. Li Y, Mathis A, Grewe BF, Osterhout JA, Ahanonu B, Schnitzer MJ, Murthy VN, and Dulac C. (2017). Neuronal Representation of Social Information in the Medial Amygdala of Awake Behaving Mice. Cell 171, 1176–1190.e17. 10.1016/j.cell.2017.10.015. [PubMed: 29107332]
15. Hong W, Kim D-W, and Anderson DJ (2014). Antagonistic control of social versus repetitive self-grooming behaviors by separable amygdala neuronal subsets. Cell 158, 1348–1361. 10.1016/j.cell.2014.07.049. [PubMed: 25215491]
16. Yamaguchi T, Wei D, Song SC, Lim B, Tritsch NX, and Lin D. (2020). Posterior amygdala regulates sexual and aggressive behaviors in male mice. Nature Neuroscience 23, 1111–1124. 10.1038/s41593-020-0675-x. [PubMed: 32719562]
17. Wei Y-C, Wang S-R, Jiao Z-L, Zhang W, Lin J-K, Li X-Y, Li S-S, Zhang X, and Xu X-H (2018). Medial preoptic area in mice is capable of mediating sexually dimorphic behaviors regardless of gender. Nat Commun 9, 279. 10.1038/s41467-017-02648-0. [PubMed: 29348568]
18. Karigo T, Kennedy A, Yang B, Liu M, Tai D, Wahle IA, and Anderson DJ (2020). Distinct hypothalamic control of same- and opposite-sex mounting behaviour in mice. Nature, 1–6. 10.1038/s41586-020-2995-0.
19. Yang B, Karigo T, and Anderson DJ (2022). Transformations of neural representations in a social behaviour network. Nature, 1–9. 10.1038/s41586-022-05057-6.
20. Unger EK, Burke KJ, Yang CF, Bender KJ, Fuller PM, and Shah NM (2015). Medial amygdalar aromatase neurons regulate aggression in both sexes. Cell Rep 10, 453–462. 10.1016/j.celrep.2014.12.040. [PubMed: 25620703]
21. Zha X, Wang L, Jiao Z-L, Yang R-R, Xu C, and Xu X-H (2020). VMHvl-Projecting Vglut1+ Neurons in the Posterior Amygdala Gate Territorial Aggression. Cell Rep 31, 107517. 10.1016/j.celrep.2020.03.081.

22. Albert DJ, Walsh ML, Gorzalka BB, Mendelson S, and Zalys C. (1986). Intermale social aggression: Suppression by medial preoptic area lesions. Physiology & Behavior 38, 169–173. 10.1016/0031-9384(86)90151-4. [PubMed: 3797483]
23. Simon NG, Cologer-Clifford A, Lu S, McKenna SE, and Hu S. (1998). Testosterone and its metabolites modulate 5HT1A and 5HT1B agonist effects on intermale aggression. Neuroscience & Biobehavioral Reviews 23, 325–336. 10.1016/S0149-7634(98)00034-7. [PubMed: 9884126]
24. Newman SW (1999). The Medial Extended Amygdala in Male Reproductive Behavior A Node in the Mammalian Social Behavior Network. Annals of the New York Academy of Sciences 877, 242–257. 10.1111/j.1749-6632.1999.tb09271.x. [PubMed: 10415653]
25. Shivers M, and Edwards DA (1978). Hypothalamic destruction and mouse aggression. Psychobiology 6, 485–487. 10.3758/BF03326753.
26. Bermond B. (1982). Effects of medial preoptic hypothalamus anterior lesions on three kinds of behavior in the rat: Intermale aggressive, male-sexual, and mouse-killing behavior. Aggressive Behavior 8, 335–354. 10.1002/1098-2337(1982)8:4<335::AID-AB2480080403>3.0.CO;2-8.
27. Wei D, Osakada T, Guo Z, Yamaguchi T, Varshneya A, Yan R, Jiang Y, and Lin D. (2023). A hypothalamic pathway that suppresses aggression toward superior opponents. Nat Neurosci 26, 774–787. 10.1038/s41593-023-01297-5. [PubMed: 37037956]
28. O'Connell LA, and Hofmann HA (2011). The Vertebrate mesolimbic reward system and social behavior network: A comparative synthesis. Journal of Comparative Neurology 519, 3599–3639. 10.1002/cne.22735. [PubMed: 21800319]
29. Goodson JL (2005). The vertebrate social behavior network: Evolutionary themes and variations. Hormones and Behavior 48, 11–22. 10.1016/j.yhbeh.2005.02.003. [PubMed: 15885690]
30. Goodson JL, and Kingsbury MA (2013). What's in a name? Considerations of homologies and nomenclature for vertebrate social behavior networks. Hormones and Behavior 64, 103–112. 10.1016/j.yhbeh.2013.05.006. [PubMed: 23722238]
31. Valcourt RJ, and Sachs BD (1979). Penile reflexes and copulatory behavior in male rats following lesions in the bed nucleus of the stria terminalis. Brain Res. Bull. 4, 131–133. [PubMed: 466486]
32. Liu YC, Salamone JD, and Sachs BD (1997). Lesions in medial preoptic area and bed nucleus of stria terminalis: differential effects on copulatory behavior and noncontact erection in male rats. J. Neurosci. 17, 5245–5253. [PubMed: 9185562]
33. Emery DE, and Sachs BD (1976). Copulatory behavior in male rats with lesions in the bed nucleus of the stria terminalis. Physiol. Behav 17, 803–806. [PubMed: 1026988]
34. Remedios R, Kennedy A, Zelikowsky M, Grewe BF, Schnitzer MJ, and Anderson DJ (2017). Social behaviour shapes hypothalamic neural ensemble representations of conspecific sex. Nature 550, 388–392. 10.1038/nature23885. [PubMed: 29052632]
35. Stagkourakis S, Spigolon G, Liu G, and Anderson DJ (2020). Experience-dependent plasticity in an innate social behavior is mediated by hypothalamic LTP. PNAS 117, 25789–25799. 10.1073/pnas.2011782117. [PubMed: 32973099]
36. Stone C, Tomilin M, and Barker R. (1935). A comparative study of sexual drive in adult male rats as measured by direct copulatory tests and by the Columbia obstruction apparatus. Journal of Comparative Psychology 19, 215.
37. Mendelson SD, and Pfaus JG (1989). Level searching: A new assay of sexual motivation in the male rat. Physiology & Behavior 45, 337–341. 10.1016/0031-9384(89)90136-4. [PubMed: 2756020]
38. Beny-Shefer Y, Zilkha N, Lavi-Avnon Y, Bezalel N, Rogachev I, Brandis A, Dayan M, and Kimchi T. (2017). Nucleus Accumbens Dopamine Signaling Regulates Sexual Preference for Females in Male Mice. Cell Reports 21, 3079–3088. 10.1016/j.celrep.2017.11.062. [PubMed: 29241537]
39. Zhang SX, Lutas A, Yang S, Diaz A, Fluhr H, Nagel G, Gao S, and Andermann ML (2021). Hypothalamic dopamine neurons motivate mating through persistent cAMP signalling. Nature 597, 245–249. 10.1038/s41586-021-03845-0. [PubMed: 34433964]
40. Dai B, Sun F, Tong X, Ding Y, Kuang A, Osakada T, Li Y, and Lin D. (2022). Responses and functions of dopamine in nucleus accumbens core during social behaviors. Cell Reports 40, 111246. 10.1016/j.celrep.2022.111246.
41. Olds J. (1956). Pleasure Centers in the Brain. Scientific American 195, 105–117.

42. Harris JA, Hirokawa KE, Sorensen SA, Gu H, Mills M, Ng LL, Bohn P, Mortrud M, Ouellette B, Kidney J, et al. (2014). Anatomical characterization of Cre driver mice for neural circuit mapping and manipulation. Front. Neural Circuits 8. 10.3389/fncir.2014.00076.
43. Powers JB, Newman SW, and Bergondy ML (1987). MPOA and BNST lesions in male Syrian hamsters: differential effects on copulatory and chemoinvestigatory behaviors. Behav. Brain Res. 23, 181–195. [PubMed: 3555537]
44. Kondo Y, Shinoda A, Yamanouchi K, and Arai Y. (1990). Role of septum and preoptic area in regulating masculine and feminine sexual behavior in male rats. Horm Behav 24, 421–434. [PubMed: 2227853]
45. Daigle TL, Madisen L, Hage TA, Valley MT, Knoblich U, Larsen RS, Takeno MM, Huang L, Gu H, Larsen R, et al. (2018). A Suite of Transgenic Driver and Reporter Mouse Lines with Enhanced Brain-Cell-Type Targeting and Functionality. Cell 174, 465–480.e22. 10.1016/j.cell.2018.06.035. [PubMed: 30007418]
46. Wickersham IR, Lyon DC, Barnard RJO, Mori T, Finke S, Conzelmann K-K, Young JAT, and Callaway EM (2007). Monosynaptic Restriction of Transsynaptic Tracing from Single, Genetically Targeted Neurons. Neuron 53, 639–647. 10.1016/j.neuron.2007.01.033. [PubMed: 17329205]
47. Miyamichi K, Shlomai-Fuchs Y, Shu M, Weissbourd BC, Luo L, and Mizrahi A. (2013). Dissecting local circuits: parvalbumin interneurons underlie broad feedback control of olfactory bulb output. Neuron 80, 1232–1245. 10.1016/j.neuron.2013.08.027. [PubMed: 24239125]
48. Copits BA, Gowrishankar R, O'Neill PR, Li J-N, Girven KS, Yoo JJ, Meshik X, Parker KE, Spangler SM, Elerding AJ, et al. (2021). A photoswitchable GPCR-based opsin for presynaptic inhibition. Neuron 109, 1791–1809.e11. 10.1016/j.neuron.2021.04.026. [PubMed: 33979635]
49. Michael V, Goffinet J, Pearson J, Wang F, Tschida K, and Mooney R. (2020). Circuit and synaptic organization of forebrain-to-midbrain pathways that promote and suppress vocalization. eLife 9, e63493. 10.7554/eLife.63493.
50. Chen J, Markowitz JE, Lilascharoen V, Taylor S, Sheurpukdi P, Keller JA, Jensen JR, Lim BK, Datta SR, and Stowers L. (2021). Flexible scaling and persistence of social vocal communication. Nature 593, 108–113. 10.1038/s41586-021-03403-8. [PubMed: 33790464]
51. Roth BL (2016). DREADDs for Neuroscientists. Neuron 89, 683–694. 10.1016/j.neuron.2016.01.040. [PubMed: 26889809]
52. Steinhoff MS, von Mentzer B, Geppetti P, Pothoulakis C, and Bunnett NW (2014). Tachykinins and Their Receptors: Contributions to Physiological Control and the Mechanisms of Disease. Physiological Reviews 94, 265–301. 10.1152/physrev.00031.2013. [PubMed: 24382888]
53. Emson PC, Jessell T, Paxinos G, and Cuello AC (1978). Substance P in the amygdaloid complex, bed nucleus and stria terminalis of the rat brain. Brain Research 149, 97–105. 10.1016/0006-8993(78)90590-5. [PubMed: 656963]
54. Ljungdahl Å, Hökfelt T, and Nilsson G. (1978). Distribution of substance P-like immunoreactivity in the central nervous system of the rat—I. Cell bodies and nerve terminals. Neuroscience 3, 861–943. 10.1016/0306-4522(78)90116-1. [PubMed: 366451]
55. Dornan WA, and Malsbury CW (1989). Peptidergic control of male rat sexual behavior: The effects of intracerebral injections of substance P and cholecystokinin. Physiology & Behavior 46, 547–556. 10.1016/0031-9384(89)90034-6. [PubMed: 2482982]
56. Berger A, Tran AH, Dida J, Minkin S, Gerard NP, Yeomans J, and Paige CJ (2012). Diminished pheromone-induced sexual behavior in neurokinin-1 receptor deficient (TACR1(−/−)) mice. Genes Brain Behav. 11, 568–576. 10.1111/j.1601-183X.2012.00787.x. [PubMed: 22471406]
57. Yu H, Miao W, Ji E, Huang S, Jin S, Zhu X, Liu M-Z, Sun Y-G, Xu F, and Yu X. (2022). Social touch-like tactile stimulation activates a tachykinin 1-oxytocin pathway to promote social interactions. Neuron 110, 1051–1067.e7. 10.1016/j.neuron.2021.12.022. [PubMed: 35045339]
58. Francis TC, Yano H, Demarest TG, Shen H, and Bonci A. (2019). High-Frequency Activation of Nucleus Accumbens D1-MSNs Drives Excitatory Potentiation on D2-MSNs. Neuron 103, 432–444.e3. 10.1016/j.neuron.2019.05.031. [PubMed: 31221559]
59. Dasgupta A, Baby N, Krishna K, Hakim M, Wong YP, Behnisch T, Soong TW, and Sajikumar S. (2017). Substance P induces plasticity and synaptic tagging/capture in rat hippocampal area CA2. Proceedings of the National Academy of Sciences 114, E8741–E8749. 10.1073/pnas.1711267114.

60. Melani R, Von Itter R, Jing D, Koppensteiner P, and Ninan I. (2019). Opposing effects of an atypical glycinergic and substance P transmission on interpeduncular nucleus plasticity. Neuropsychopharmacol. 44, 1828–1836. 10.1038/s41386-019-0396-6.
61. Masterson SP, Li J, and Bickford ME (2010). Frequency-Dependent Release of Substance P Mediates Heterosynaptic Potentiation of Glutamatergic Synaptic Responses in the Rat Visual Thalamus. Journal of Neurophysiology 104, 1758–1767. 10.1152/jn.00010.2010. [PubMed: 20660425]
62. Cascieri MA, Ber E, Fong TM, Sadowski S, Bansal A, Swain C, Seward E, Frances B, Burns D, and Strader CD (1992). Characterization of the binding of a potent, selective, radioiodinated antagonist to the human neurokinin-1 receptor. Mol Pharmacol 42, 458–463. [PubMed: 1383685]
63. Malenka RC, Kauer JA, Zucker RS, and Nicoll RA (1988). Postsynaptic Calcium Is Sufficient for Potentiation of Hippocampal Synaptic Transmission. Science 242, 81–84. 10.1126/science.2845577. [PubMed: 2845577]
64. Weisskopf MG, and Nicoll RA (1995). Presynaptic changes during mossy fibre LTP revealed by NMDA receptor-mediated synaptic responses. Nature 376, 256–259. 10.1038/376256a0. [PubMed: 7617037]
65. Salin PA, Malenka RC, and Nicoll RA (1996). Cyclic AMP Mediates a Presynaptic Form of LTP at Cerebellar Parallel Fiber Synapses. Neuron 16, 797–803. 10.1016/S0896-6273(00)80099-9. [PubMed: 8607997]
66. Hökfelt T, Broberger C, Xu Z-QD, Sergeyev V, Ubink R, and Diez M. (2000). Neuropeptides — an overview. Neuropharmacology 39, 1337–1356. 10.1016/S0028-3908(00)00010-1. [PubMed: 10818251]
67. Mcgill TE, and Blight WC (1963). Effects of genotype on the recovery of sex drive in the male mouse. J Comp Physiol Psychol 56, 887–888. 10.1037/h0044719. [PubMed: 14050181]
68. McGill TE, and Tucker GR (1964). Genotype and sex drive in intact and in castrated male mice. Science 145, 514–515. [PubMed: 14163780]
69. Malsbury CW (1971). Facilitation of male rat copulatory behavior by electrical stimulation of the medial preoptic area. Physiology & Behavior 7, 797–805. 10.1016/0031-9384(71)90042-4. [PubMed: 5134017]
70. Moffitt JR, Bambah-Mukku D, Eichhorn SW, Vaughn E, Shekhar K, Perez JD, Rubinstein ND, Hao J, Regev A, Dulac C, et al. (2018). Molecular, spatial, and functional single-cell profiling of the hypothalamic preoptic region. Science 362. 10.1126/science.aau5324.
71. Olds J. (1958). Self-Stimulation of the Brain. Science 127, 315–324. 10.1126/science.127.3294.315. [PubMed: 13506579]
72. Olds J. (1956). A preliminary mapping of electrical reinforcing effects in the rat brain. J Comp Physiol Psychol 49, 281–285. 10.1037/h0041287. [PubMed: 13332128]
73. Szabó I. (1973). Path neuron system of medial forebrain bundle as a possible substrate for hypothalamic self-stimulation. Physiology & Behavior 10, 315–328. 10.1016/00319384(73)90316-8. [PubMed: 4350732]
74. Muñoz C, Keller I, and Huston JP (1985). Evidence for a role of the preoptic area in lateral hypothalamic self-stimulation. Brain Research 358, 85–95. 10.1016/0006-8993(85)90951-5. [PubMed: 4075134]
75. van de Poll NE, and van Dis H. (1971). Sexual motivation and medial preoptic self-stimulation in male rats. Psychon Sci 25, 137–138. 10.3758/BF03332475.
76. Tan H-E, Sisti AC, Jin H, Vignovich M, Villavicencio M, Tsang KS, Goffer Y, and Zuker CS (2020). The gut-brain axis mediates sugar preference. Nature 580, 511–516. 10.1038/s41586-020-2199-7. [PubMed: 32322067]
77. Zhou X, Li A, Mi X, Li Y, Ding Z, An M, Chen Y, Li W, Tao X, Chen X, et al. (2023). Hyperexcited limbic neurons represent sexual satiety and reduce mating motivation. Science 379, 820–825. 10.1126/science.abl4038. [PubMed: 36758107]
78. Wise RA (2004). Dopamine, learning and motivation. Nat Rev Neurosci 5, 483–494. 10.1038/nrn1406. [PubMed: 15152198]
79. Dulac C, and Wagner S. (2006). Genetic analysis of brain circuits underlying pheromone signaling. Annu. Rev. Genet. 40, 449–467. 10.1146/annurev.genet.39.073003.093937. [PubMed: 16953793]

80. Broadwell RD (1975). Olfactory relationships of the telencephalon and diencephalon in the rabbit. I. An autoradiographic study of the efferent connections of the main and accessory olfactory bulbs. J. Comp. Neurol. 163, 329–345. 10.1002/cne.901630306. [PubMed: 1176643]
81. Scalia F, and Winans SS (1975). The differential projections of the olfactory bulb and accessory olfactory bulb in mammals. J. Comp. Neurol. 161, 31–55. 10.1002/cne.901610105. [PubMed: 1133226]
82. Dederen PJ, Gribnau AA, and Curfs MH (1994). Retrograde neuronal tracing with cholera toxin B subunit: comparison of three different visualization methods. Histochem J 26, 856–862. 10.1007/BF00162931. [PubMed: 7868356]
83. Schneider DM, Nelson A, and Mooney R. (2014). A synaptic and circuit basis for corollary discharge in the auditory cortex. Nature 513, 189–194. 10.1038/nature13724. [PubMed: 25162524]
84. Wersinger SR, and Rissman EF (2000). Dopamine Activates Masculine Sexual Behavior Independent of the Estrogen Receptor α. J. Neurosci. 20, 4248–4254. 10.1523/JNEUROSCI.20-11-04248.2000. [PubMed: 10818161]
85. Haglund L, Köhler C, Ross SB, and Kelder D. (1979). Forebrain projections of the ventral tegmentum as studied by axonal transport of [3H]dopamine in the rat. Neuroscience Letters 12, 301–306. 10.1016/0304-3940(79)96079-8. [PubMed: 88699]
86. Sun F, Zhou J, Dai B, Qian T, Zeng J, Li X, Zhuo Y, Zhang Y, Wang Y, Qian C, et al. (2020). Next-generation GRAB sensors for monitoring dopaminergic activity in vivo. Nat Methods 17, 1156–1166. 10.1038/s41592-020-00981-9. [PubMed: 33087905]
87. Nyby J, Dizinno GA, and Whitney G. (1976). Social status and ultrasonic vocalizations of male mice. Behavioral Biology 18, 285–289. 10.1016/S0091-6773(76)92198-2. [PubMed: 999582]
88. Lumley LA, Sipos ML, Charles RC, Charles RF, and Meyerhoff JL (1999). Social Stress Effects on Territorial Marking and Ultrasonic Vocalizations in Mice. Physiology & Behavior 67, 769–775. 10.1016/S0031-9384(99)00131-6. [PubMed: 10604849]
89. Chabout J, Serreau P, Ey E, Bellier L, Aubin T, Bourgeron T, and Granon S. (2012). Adult Male Mice Emit Context-Specific Ultrasonic Vocalizations That Are Modulated by Prior Isolation or Group Rearing Environment. PLOS ONE 7, e29401. 10.1371/journal.pone.0029401.
90. Faure A, Pittaras E, Nosjean A, Chabout J, Cressant A, and Granon S. (2017). Social behaviors and acoustic vocalizations in different strains of mice. Behavioural Brain Research 320, 383–390. 10.1016/j.bbr.2016.11.003. [PubMed: 27825934]
91. Schmidt M, Lapert F, Brandwein C, Deuschle M, Kasperk C, Grimsley JM, and Gass P. (2017). Prenatal stress changes courtship vocalizations and bone mineral density in mice. Psychoneuroendocrinology 75, 203–212. 10.1016/j.psyneuen.2016.11.003. [PubMed: 27838514]
92. Lischinsky JE, and Lin D. (2020). Neural mechanisms of aggression across species. Nat Neurosci 23, 1317–1328. 10.1038/s41593-020-00715-2. [PubMed: 33046890]
93. Stagkourakis S, Spigolon G, Williams P, Protzmann J, Fisone G, and Broberger C. (2018). A neural network for intermale aggression to establish social hierarchy. Nat Neurosci 21, 834–842. 10.1038/s41593-018-0153-x. [PubMed: 29802391]
94. Kohl J, Babayan BM, Rubinstein ND, Autry AE, Marin-Rodriguez B, Kapoor V, Miyamishi K, Zweifel LS, Luo L, Uchida N, et al. (2018). Functional circuit architecture underlying parental behaviour. Nature 556, 326–331. 10.1038/s41586-018-0027-0. [PubMed: 29643503]
95. Agmo A, and Berenfeld R. (1990). Reinforcing Properties of Ejaculation in the Male Rat: Role of Opioids and Dopamine. Behavioral Neuroscience 104, 177–182. 10.1037//0735-7044.104.1.177. [PubMed: 2156520]
96. Olds J, and Milner P. (1954). Positive reinforcement produced by electrical stimulation of septal area and other regions of rat brain. J Comp Physiol Psychol 47, 419–427. 10.1037/h0058775. [PubMed: 13233369]
97. McHenry JA, Otis JM, Rossi MA, Robinson JE, Kosyk O, Miller NW, McElligott ZA, Budygin EA, Rubinow DR, and Stuber GD (2017). Hormonal gain control of a medial preoptic area social reward circuit. Nat Neurosci 20, 449–458. 10.1038/nn.4487. [PubMed: 28135243]

98. Hung LW, Neuner S, Polepalli JS, Beier KT, Wright M, Walsh JJ, Lewis EM, Luo L, Deisseroth K, Dölen G, et al. (2017). Gating of social reward by oxytocin in the ventral tegmental area. Science 357, 1406–1411. 10.1126/science.aan4994. [PubMed: 28963257]

99. Dölen G, Darvishzadeh A, Huang KW, and Malenka RC (2013). Social reward requires coordinated activity of nucleus accumbens oxytocin and serotonin. Nature 501, 179–184. 10.1038/nature12518. [PubMed: 24025838]

100. Betley JN, Xu S, Cao ZFH, Gong R, Magnus CJ, Yu Y, and Sternson SM (2015). Neurons for hunger and thirst transmit a negative-valence teaching signal. Nature 521, 180–185. 10.1038/nature14416. [PubMed: 25915020]

101. Allen WE, DeNardo LA, Chen MZ, Liu CD, Loh KM, Fenno LE, Ramakrishnan C, Deisseroth K, and Luo L. (2017). Thirst-associated preoptic neurons encode an aversive motivational drive. Science 357, 1149–1155. 10.1126/science.aan6747. [PubMed: 28912243]

102. Chen Y, Lin Y-C, Zimmerman CA, Essner RA, and Knight ZA (2016). Hunger neurons drive feeding through a sustained, positive reinforcement signal. eLife 5, e18640. 10.7554/eLife.18640.

103. Augustine V, Ebisu H, Zhao Y, Lee S, Ho B, Mizuno GO, Tian L, and Oka Y. (2019). Temporally and Spatially Distinct Thirst Satiation Signals. Neuron 103, 242–249.e4. 10.1016/j.neuron.2019.04.039. [PubMed: 31153646]

104. Jennings JH, Ung RL, Resendez SL, Stamatakis AM, Taylor JG, Huang J, Veleta K, Kantak PA, Aita M, Shilling-Scrivo K, et al. (2015). Visualizing hypothalamic network dynamics for appetitive and consummatory behaviors. Cell 160, 516–527. 10.1016/j.cell.2014.12.026. [PubMed: 25635459]

105. Leib DE, Zimmerman CA, Poormoghaddam A, Huey EL, Ahn JS, Lin Y-C, Tan CL, Chen Y, and Knight ZA (2017). The Forebrain Thirst Circuit Drives Drinking through Negative Reinforcement. Neuron 96, 1272–1281.e4. 10.1016/j.neuron.2017.11.041. [PubMed: 29268095]

106. Augustine V, Lee S, and Oka Y. (2020). Neural Control and Modulation of Thirst, Sodium Appetite, and Hunger. Cell 180, 25–32. 10.1016/j.cell.2019.11.040. [PubMed: 31923398]

107. Perachio AA, Marr LD, and Alexander M. (1979). Sexual behavior in male rhesus monkeys elicited by electrical stimulation of preoptic and hypothalamic areas. Brain Research 177, 127–144. 10.1016/0006-8993(79)90923-5. [PubMed: 115544]

108. Robinson BW, and Mishkin M. (1966). Ejaculation evoked by stimulation of the preoptic area in monkey. Physiology & Behavior 1, 269-IN11. 10.1016/0031-9384(66)90016-3.

109. Oomura Y, Yoshimatsu H, and Aou S. (1983). Medial preoptic and hypothalamic neuronal activity during sexual behavior of the male monkey. Brain Res. 266, 340–343. [PubMed: 6871668]

110. Ghofrani HA, Osterloh IH, and Grimminger F. (2006). Sildenafil: from angina to erectile dysfunction to pulmonary hypertension and beyond. Nat Rev Drug Discov 5, 689–702. 10.1038/nrd2030. [PubMed: 16883306]

111. Paxinos G, and Franklin KBJ (2003). The Mouse Brain in Stereotaxic Coordinates: Compact Second Edition, Second Edition 2nd ed. (Academic Press).

112. Cao YQ, Mantyh PW, Carlson EJ, Gillespie A-M, Epstein CJ, and Basbaum AI (1998). Primary afferent tachykinins are required to experience moderate to intense pain. Nature 392, 390–394. 10.1038/32897. [PubMed: 9537322]

113. Inoue S, Yang R, Tantry A, Davis C-H, Yang T, Knoedler JR, Wei Y, Adams EL, Thombare S, Golf SR, et al. (2019). Periodic Remodeling in a Neural Circuit Governs Timing of Female Sexual Behavior. Cell 179, 1393–1408.e16. 10.1016/j.cell.2019.10.025. [PubMed: 31735496]

114. Ebner K, Rupniak NM, Saria A, and Singewald N. (2004). Substance P in the medial amygdala: Emotional stress-sensitive release and modulation of anxiety-related behavior in rats. Proceedings of the National Academy of Sciences 101, 4280–4285. 10.1073/pnas.0400794101.

115. Gavioli EC, Canteras NS, and De Lima TCM (2002). The role of lateral septal NK1 receptors in mediating anxiogenic effects induced by intracerebroventricular injection of substance P. Behavioural Brain Research 134, 411–415. 10.1016/S0166-4328(02)00054-2.

116. Scott N, Prigge M, Yizhar O, and Kimchi T. (2015). A sexually dimorphic hypothalamic circuit controls maternal care and oxytocin secretion. Nature 525, 519–522. 10.1038/nature15378. [PubMed: 26375004]

117. Zhou P, Resendez SL, Rodriguez-Romaguera J, Jimenez JC, Neufeld SQ, Giovannucci A, Friedrich J, Pnevmatikakis EA, Stuber GD, Hen R, et al. (2018). Efficient and accurate extraction of in vivo calcium signals from microendoscopic video data. Elife 7. 10.7554/eLife.28728.

118. Wu MV, Manoli DS, Fraser EJ, Coats JK, Tollkuhn J, Honda S-I, Harada N, and Shah NM (2009). Estrogen masculinizes neural pathways and sex-specific behaviors. Cell 139, 61–72. 10.1016/j.cell.2009.07.036. [PubMed: 19804754]

119. Xu X, Coats JK, Yang CF, Wang A, Ahmed OM, Alvarado M, Izumi T, and Shah NM (2012). Modular genetic control of sexually dimorphic behaviors. Cell 148, 596–607. 10.1016/j.cell.2011.12.018. [PubMed: 22304924]

120. Juntti SA, Tollkuhn J, Wu MV, Fraser EJ, Soderborg T, Tan S, Honda S-I, Harada N, and Shah NM (2010). The androgen receptor governs the execution, but not programming, of male sexual and territorial behaviors. Neuron 66, 260–272. 10.1016/j.neuron.2010.03.024. [PubMed: 20435002]

121. Yang T, Bayless DW, Wei Y, Landayan D, Marcelo IM, Wang Y, DeNardo LA, Luo L, Druckmann S, and Shah NM (2023). Hypothalamic neurons that mirror aggression. Cell 186, 1195–1211.e19. 10.1016/j.cell.2023.01.022. [PubMed: 36796363]

Highlights

- A multisynaptic neural circuit that converts sensory input to male sexual behavior.
- An embedded molecular timer delays mating onset following mate-recognition.
- This neural circuit elicits dopamine release and governs male sexual drive and reward.
- This neural circuit governs libido and motor displays of male sexual behavior.

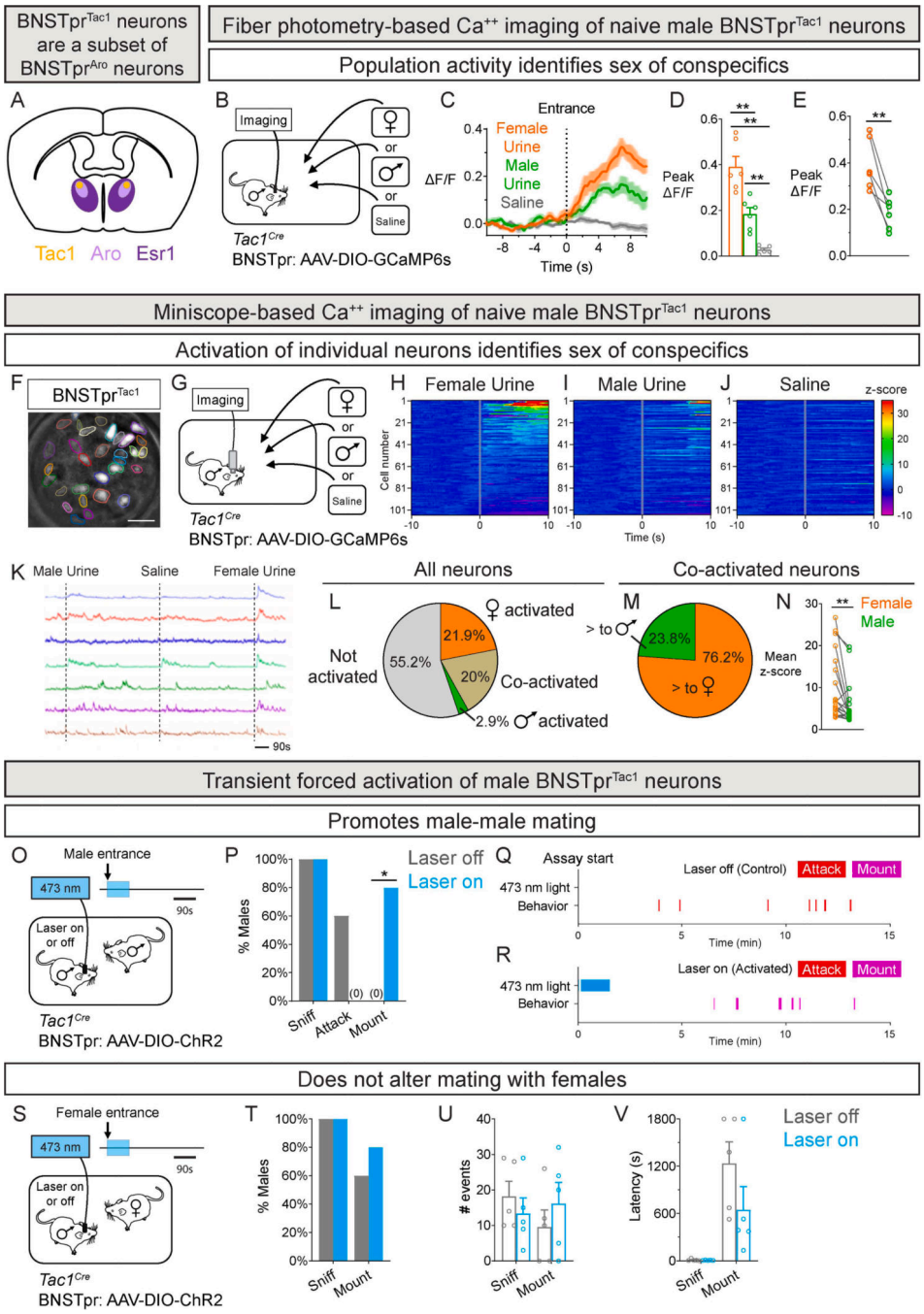

Figure 1: Activity of male BNSTpr^{Tac1} neurons identifies sex of conspecifics and promotes mating.

A. Schematic of section through the adult mouse brain showing that BNSTpr^{Tac1} neurons are a subset of BNSTpr^{Aro} neurons, which are a subset of BNSTpr^{Esr1} neurons.

B-E. Schematic of fiber photometry of BNSTpr^{Tac1} neurons in males investigating swabs wetted with female urine, male urine, or saline (B). Peri-event time plot (PETP) of normalized GCaMP6s fluorescence (ΔF/F; dark line, mean, and shaded area, SEM for all Figure panels with fiber photometry; dashed vertical line marks insertion of swab into the

cage) (C). BNSTpr^{Tac1} neurons are activated by urine (D), with larger response to female than male urine (E).

F-J. GRIN lens imaging of BSNTpr^{Tac1} GCaMP6s fluorescence with segmented neurons (F). Schematic of miniscope imaging of BNSTpr^{Tac1} neurons in males investigating swabs as in panel B (G). Heatmaps of activation of individual neurons during presentation of urine or saline; row numbers correspond to the same neuron across panels, with rows sorted by activation to female urine (H-J).

K-N. Traces of GCaMP6s fluorescence (ΔF/F) of individual neurons in response to stimulus presentation (dashed lines) (K). Percent neurons activated by female or male urine or both (L). Percent co-activated neurons with differential response to female or male urine (M). Among co-activated neurons, the response to female urine was greater than that to male urine (N). Neurons were classified as activated if the peak z-score during the 10s period following swab insertion was >2σ of the peak z-score during the 10s period preceding swab insertion.

O-R. Schematic of optogenetic activation of BNSTpr^{Tac1} neurons of a resident male interacting with an intruder male (O). Activation during the first 90s eliminates attacks and promotes mating (P). Raster plot of a male showing aggression toward the intruder without optogenetic activation (Q). Raster plot of behavior of male showing mating with the intruder following optogenetic activation (R).

S-V. Schematic of optogenetic activation of BNSTpr^{Tac1} neurons of a resident male interacting with intruder female (S). Optogenetic activation of these cells during the first 90s does not alter the probability (T), number (U), or latency (V) of sniffing or mounting. Mean ± SEM. n = 6 mice (B-E), 105 neurons from 3 mice (F-N), and 5 mice (O-V). * $p < 0.05$, ** $p < 0.01$. Scale bar = 100 μm (F).

See also Fig. S1; Tables S1-3.

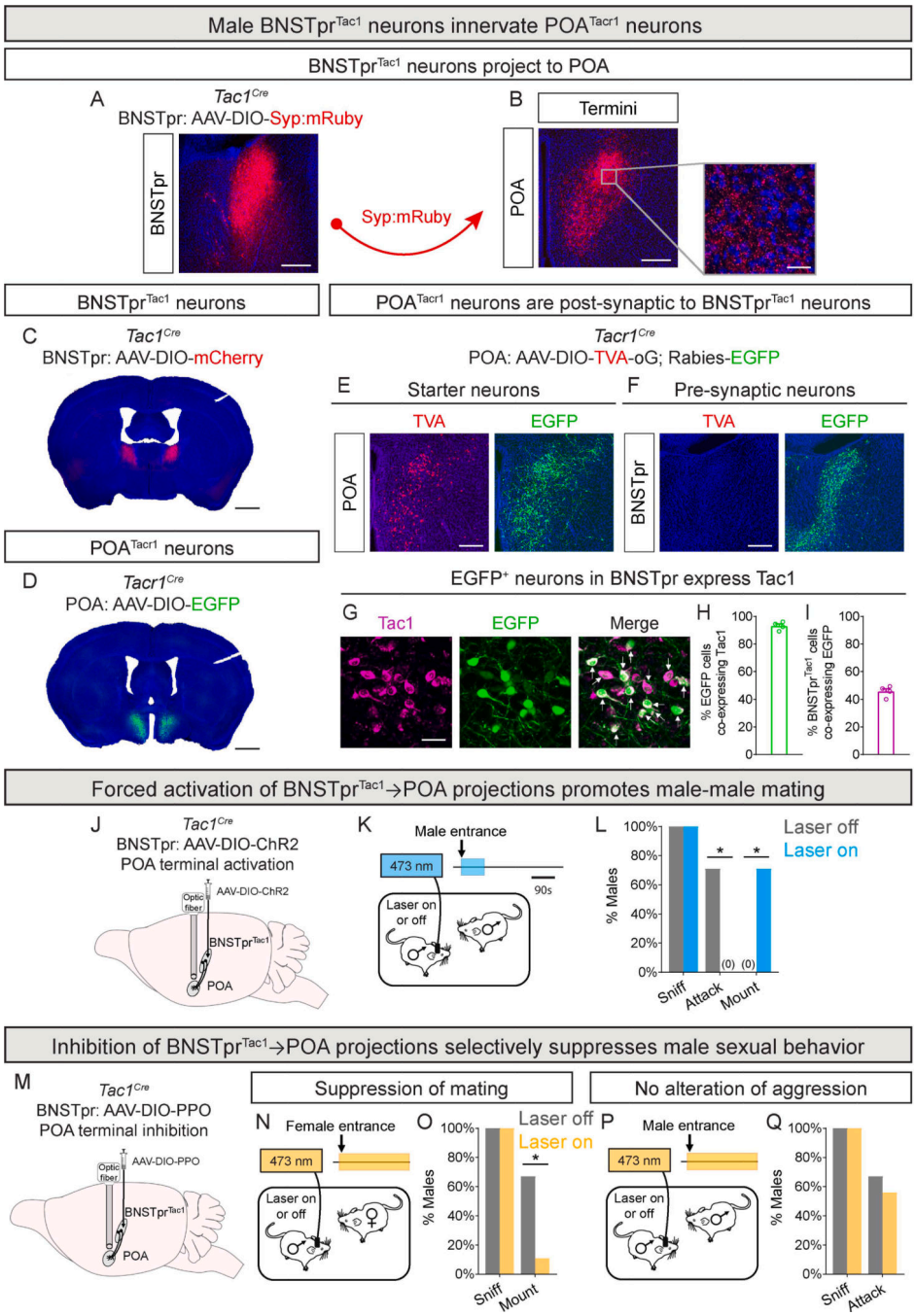

Figure 2: Innervation of POA^{Tacr1} neurons by BNSTpr^{Tac1} neurons is essential for male mating.

A-B. Syp:mRuby expression in BNSTpr^{Tac1} neurons (A). Syp:mRuby+ termini of BNSTpr^{Tac1} neurons in the POA; inset shows area boxed in gray (B).

C-D. mCherry+ BNSTpr^{Tac1} neurons (C) and EGFP+ POA^{Tacr1} neurons (D) visualized in coronal sections.

E-I. TVA (mCherry) and Rabies (EGFP) expression in POA^{Tacr1} starter neurons (E). EGFP+ and TVA–BNSTpr neurons innervating POA^{Tacr1} neurons (F). Co-labeling for Tac1 mRNA and EGFP in BNSTpr neurons innervating POA^{Tacr1} neurons; arrows show Tac1+, EGFP+

cells (G). Most BNSTpr neurons presynaptic to POA^{Tacr1} neurons are BNSTpr^{Tac1} neurons (H), and nearly half of BNSTpr^{Tac1} neurons innervate POA^{Tacr1} neurons (I).

J-L. Strategy to activate BNSTpr^{Tac1}→POA projections (J). Schematic of optogenetic activation of BNSTpr^{Tac1}→POA projections of a resident male interacting with intruder male (K). Activation during the first 90s eliminates attacks and promotes mating (L).

M-Q. Strategy to inhibit BNSTpr^{Tac1}→POA projections (M). Schematic of optogenetic inhibition of BNSTpr^{Tac1}→POA projections of a resident male interacting with intruder female (N) or male (P). Inhibition suppresses mating with females (O) but does not alter aggression toward males (Q).

Mean ± SEM. n = 4 (A-I), 7 (J-L), and 9 (M-Q) mice. * $p < 0.05$. Scale bars = 1 mm (C,D), 200 μm (A,B,E,F), 20 μm (B inset, G).

See also Fig. S2; Tables S1,3.

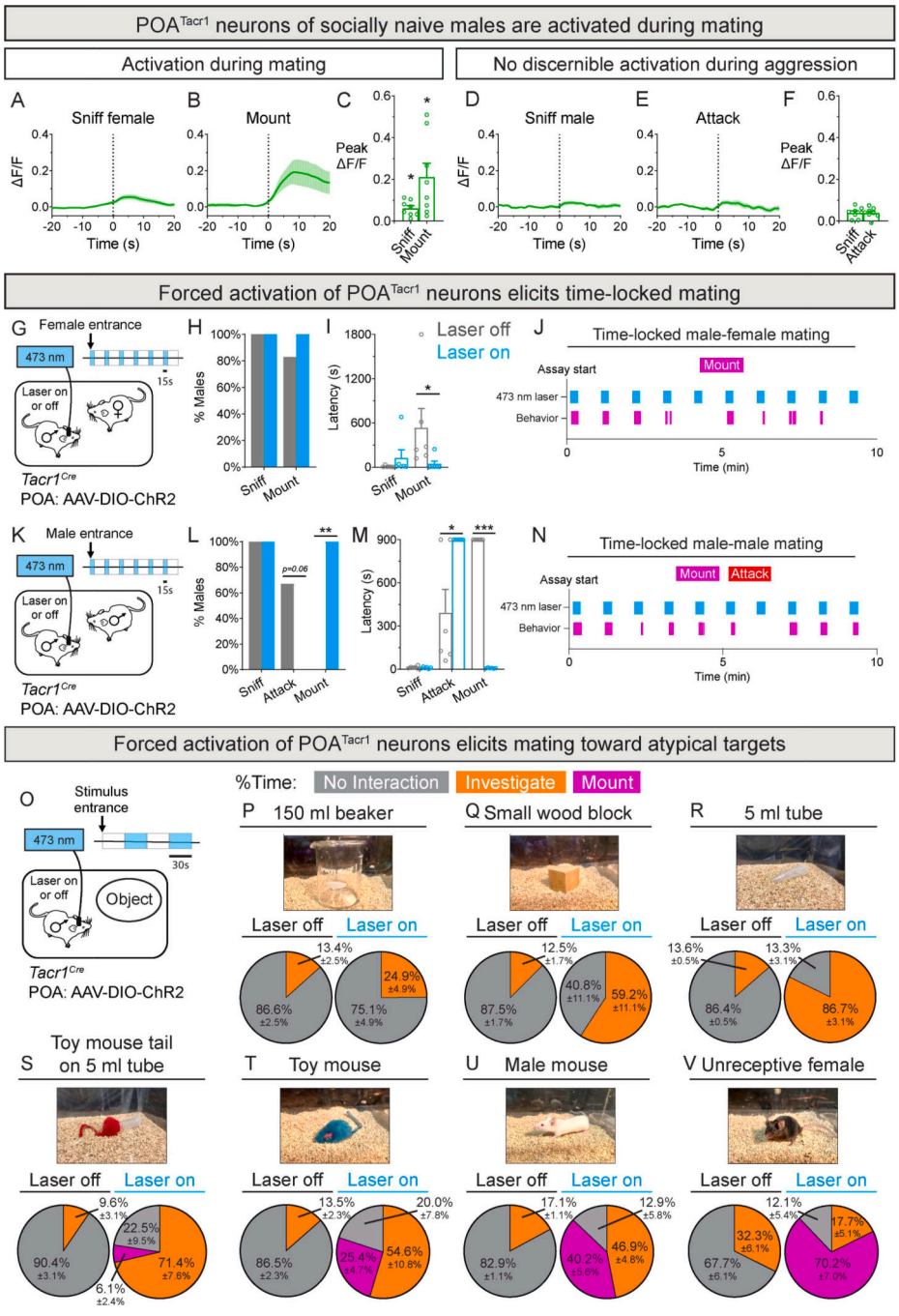

Figure 3: POA^{Tacr1} neurons are active during male mating and drive male sexual behavior.

A-C. Fiber photometry of POA^{Tacr1} neurons in males interacting with intruder female. PETP of GCaMP6s fluorescence (ΔF/F) during sniffing (A) and mounting (B). BNSTpr^{Tac1} neurons are activated during sniffs and mounts (C).

D-F. Fiber photometry of POA^{Tacr1} neurons in males interacting with intruder male. PETP of GCaMP6s fluorescence (ΔF/F) during sniffing (D) and attacks (E). No discernible activation of BNSTpr^{Tac1} neurons during sniffs or attacks (F).

G-J. Schematic of optogenetic activation of POA^{Tacr1} neurons of males interacting with females (G). Activation (15/45 s on/off) does not alter percent males mounting females (H) but reduces mating latency ~100-fold (I). Raster plot shows male mounting time-locked to light.

K-N. Schematic of optogenetic activation of POA^{Tacr1} neurons of males interacting with intruder males (K). Activation (15/45 s on/off) abrogates aggression and elicits mating (L). Fight latency is prolonged whereas mating latency is reduced by ≥100-fold (M). Raster plot shows male mounting time-locked to light (N).

O-V. Schematic of optogenetic activation (30/30 s on/off; 2 min encounter) of POA^{Tacr1} neurons of males interacting with inanimate objects (O). Activation progressively increased investigation of a beaker (P), wood block (Q), and tube (R) and elicited mounting toward the tube outfitted with a toy mouse tail (S), toy mouse (T), male (U), and an unreceptive female (V).

Mean (dark trace) ± SEM (lighter shading) of GCaMP6s activity shown in PETPs of all Figures. Mean ± SEM. n = 8 (A-F), 6 (G-N), and 4 (O-V) mice. * $p < 0.05$, *** $p < 0.001$. See also Fig. S3; Tables S1,3,4; Movie S1.

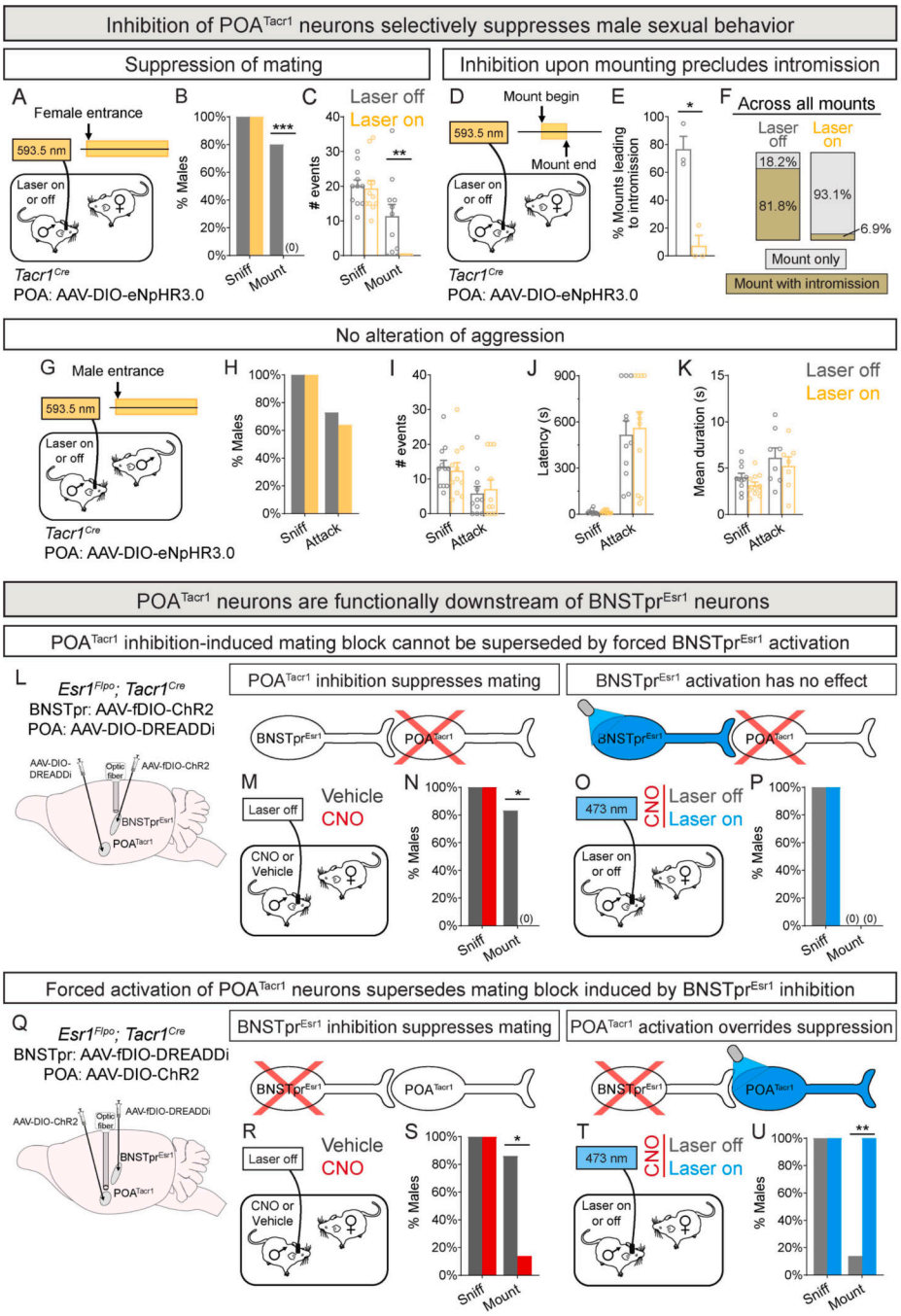

Figure 4: POA^{Tacr1} neurons are functionally downstream of BNSTpr^{Esr1} neurons for male mating.

A-C. Schematic of optogenetic inhibition of POA^{Tacr1} neurons in males interacting with intruder females (A). Silencing eliminates mounting without altering sniffing (B,C).

D-F. Schematic of closed-loop optogenetic inhibition of POA^{Tacr1} neurons during mounting (D). Silencing reduced transitions from mount to intromission (E,F). n = 44 mounts (F, laser off), 29 mounts (F, laser on).

G-K. Schematic of optogenetic inhibition of POA^{Tacr1} neurons in males interacting with intruder males (G). Silencing did not alter the probability (H), number (I), latency (J), or duration (K) of attacks.

L-P. Strategy to activate BNSTpr^{Esr1} neurons while inhibiting POA^{Tacr1} neurons (L). Schematic of chemogenetic inhibition of POA^{Tacr1} neurons in males (red cross over POA^{Tacr1} neurons in circuit models above M-P) interacting with females (M). Inhibition of POA^{Tacr1} neurons eliminates mating (N). Schematic of optogenetic activation of BNSTpr^{Esr1} neurons (shaded blue in circuit model above O-P) in males given CNO and interacting with females (O). Inhibition of POA^{Tacr1} neurons eliminated mating even when BNSTpr^{Esr1} neurons were activated (P).

Q-U. Strategy to activate POA^{Tacr1} neurons while inhibiting BNSTpr^{Esr1} neurons (Q). Schematic of chemogenetic inhibition of BNSTpr^{Esr1} neurons (red cross over BNSTpr neurons in circuit models above R-U) in males interacting with females (R). Inhibition of BNSTpr^{Esr1} neurons suppressed mating (S). Schematic of optogenetic activation of POA^{Tacr1} neurons (shaded blue in circuit model above TU) in males given CNO and interacting with females (T). Activation of POA^{Tacr1} neurons induced mating even when BNSTpr^{Esr1} neurons were inhibited (U).

Mean ± SEM. n = 11 (A-C), 3 (D-F), 11 (G-K), 6 (L-P) and 7 (Q-U) mice. * $p < 0.05$, ** $p < 0.01$.

See also Fig. S3,4; Tables S1,3.

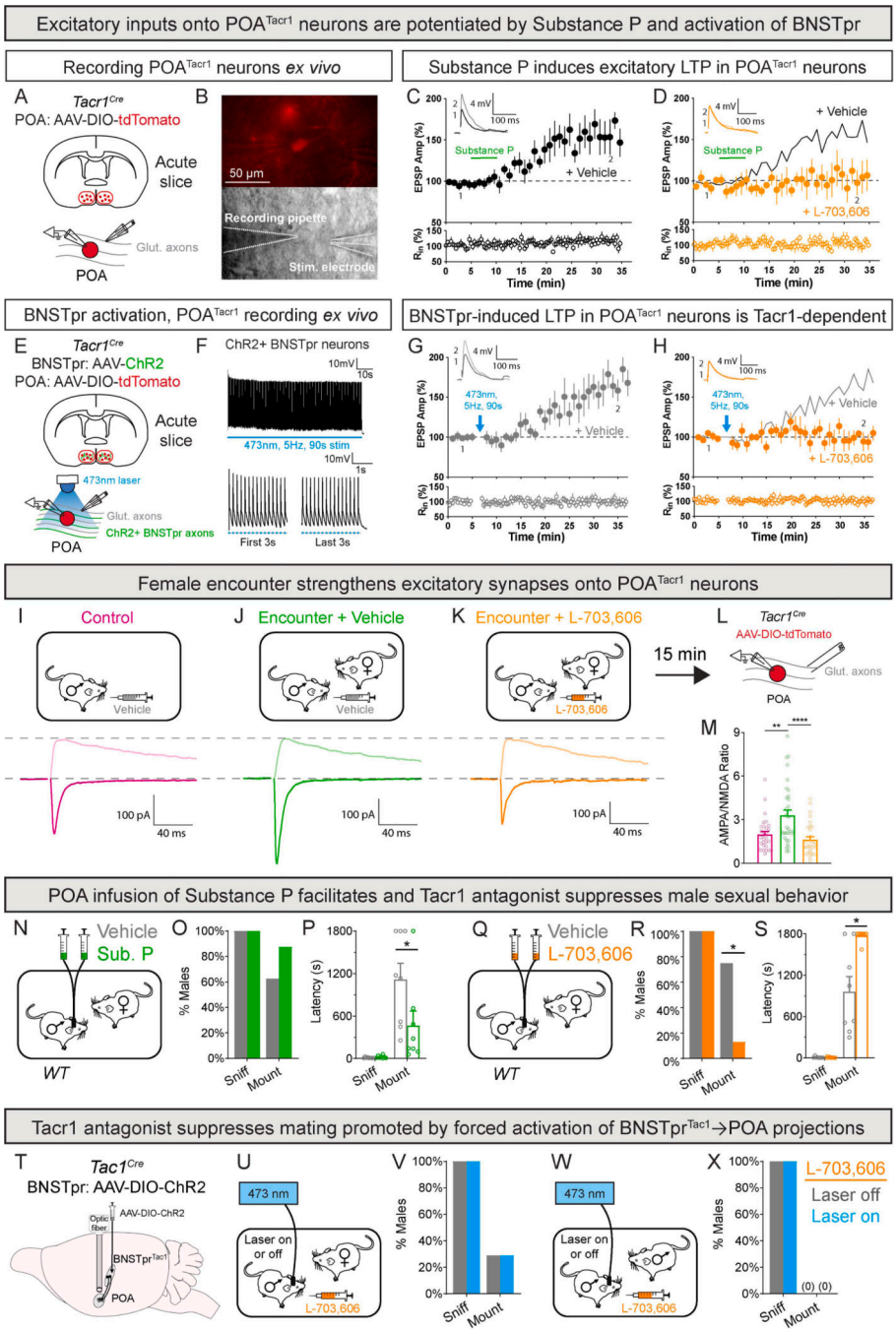

Figure 5: Substance P-Tacr1 signaling potentiates activation of POA^{Tacr1} neurons and promotes male mating

A-D. Substance P induces LTP in POA^{Tacr1} neurons.

Strategy to record POA^{Tacr1} neurons with local stimulation of glutamatergic inputs in the presence of picrotoxin (100 µM) (A).

tdTomato+ POA^{Tacr1} neurons (upper) and recording pipette and theta stimulation electrode (lower) (B).

Summary plot of normalized EPSP amplitudes (Amp) and input resistance (R_{in}) before and after 5 min (green line) bath application of Substance P (50nM). Inset: Representative EPSP traces of baseline (1) and the last 5 min (2) (C-D).

Substance P induces LTP in POA^{Tacr1} neurons (C) and the Tacr1 antagonist L-703,606 (10 μM for slice recordings) blocks it (D). Black line (D) represents average trace with vehicle.

E-H. Activation of BNSTpr projections induces LTP onto POA^{Tacr1} neurons.

Strategy to record POA^{Tacr1} neurons while optogenetically activating BNSTpr→POA projections in the presence of picrotoxin (E).

Trace of light-evoked firing of BNSTpr neurons (F, upper). Light elicits reliable firing early as well as later (F, lower).

Summary plot of normalized EPSP Amp and R_{in} before and after transient activation (90 s, blue arrow) of BNSTpr→POA projections (G-H). Inset: Representative EPSP traces of baseline (1) and the last 5 min (2) (G-H).

Light induces LTP in POA^{Tacr1} neurons (G) and L-703,606 blocks it (H). Gray line (H) represents the average trace with vehicle.

I-M. Female encounter strengthens excitatory synapses onto POA^{Tacr1} neurons in a Substance P-dependent manner.

Schematic of assay in which singly-housed males were administered vehicle or L-703,606 (10 mg/kg for *in vivo* studies) 30 min prior to initiating testing (I-K, upper panels), and strategy to record POA^{Tacr1} neurons with local stimulation of glutamatergic inputs in the presence of picrotoxin (L).

Darker and lighter traces show example excitatory postsynaptic currents recorded at −70 mV and +40 mV, respectively (I-K, lower panels).

MPA/NMDA ratio is increased only in males given vehicle prior to encountering a female (M).

N-P. Schematic of paradigm to infuse Substance P into the POA of WT males interacting with females. Substance P (10 ng in 200 nL) or vehicle was infused 15 min prior to female entry. Substance P did not alter probability of (O) but reduced latency to initiate (P) mating.

Q-S. Schematic of infusion of L-703,606 (500 pmol in 200 nL) into the POA of WT males interacting with a receptive female (Q). L-703,606 reduced the probability of (R) and increased latency to initiate (S) mating.

T-X. Strategy to activate BNSTpr^{Tac1}→POA projections (T). Schematic of optogenetic activation of BNSTpr^{Tac1}→POA projections in males given L-703,606 and interacting with females (U). L-703,606 suppresses mating even upon activation of BNSTpr^{Tac1}→POA projections (V). Schematic of optogenetic activation of BNSTpr^{Tac1}→POA projections in males given L-703,606 and interacting with males (W). L-703,606 eliminates the male-male mating promoted by activation of BNSTpr^{Tac1}→POA projections (X).

Mean ± SEM. n = 7 neurons from 4 mice (C), 5 neurons from 3 mice (D), 8 neurons from 4 mice (G), 7 neurons from 3 mice (H), 30 neurons from 4 mice (Control), 33 neurons from 5 mice (Encounter + Vehicle), 31 neurons from 4 mice (Encounter + L-703,606) (M), 8 mice (N-S), 7 mice (T-X). * $p < 0.05$, ** $p < 0.01$, **** $p < 0.0001$.

See also Fig. S5,6; Tables S1,3.

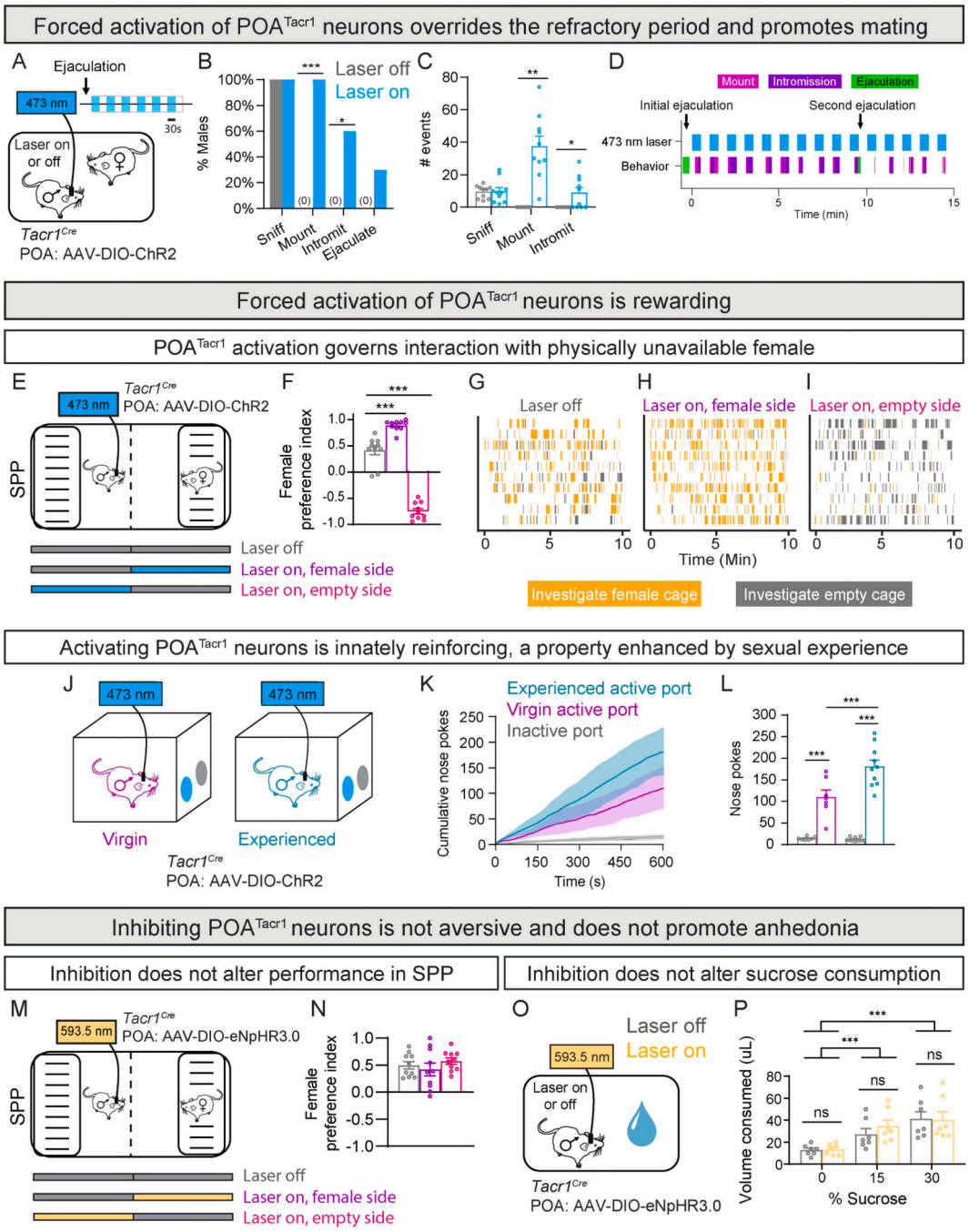

Figure 6: Forced activation of POA^{Tacr1} neuron overrides the post-ejaculatory refractory period and is self-reinforcing.

A-D. Schematic of optogenetic activation of POA^{Tacr1} neurons in post-ejaculatory males interacting with females (A). Activation (30/30 s on/off) of these cells re-ignites mating drive, increasing the probability (B) and number (C) of mating routines. Raster plot of sexually satiated male subsequent to activating POA^{Tacr1} neurons (D).

E-I. Schematic of optogenetic activation of POA^{Tacr1} neurons in the SPP test (E). Activation governs behavioral preference of males (F). Raster plots (each row is a male) showing that optogenetic activation governs investigation by males (H-I).
J-L. Schematic of optogenetic self-stimulation (0.5 s, 40 Hz) of POA^{Tacr1} neurons in virgin and sexually experienced males (J). Both virgin and experienced males show more nose pokes to the active port (K,L), with sexual experience increasing self-stimulation (L).
M-N. Schematic of optogenetic inhibition of POA^{Tacr1} neurons during the SPP test (M). Inhibition does not alter male preference for side containing the female (N).
O-P. Schematic of optogenetic inhibition of POA^{Tacr1} neurons during sucrose consumption test (O). Inhibition does not alter sucrose consumption (P).
Mean ± SEM. n = 10 mice (A-D), n = 10 mice (E-I), n = 7 virgin mice and 10 experienced mice (J-L), n = 10 mice (M-N), n = 6 mice (O-P). * $p < 0.05$, ** $p < 0.01$, *** $p < 0.001$.
See also Fig. S7; Tables S1,3; Data S1; Movie S2.

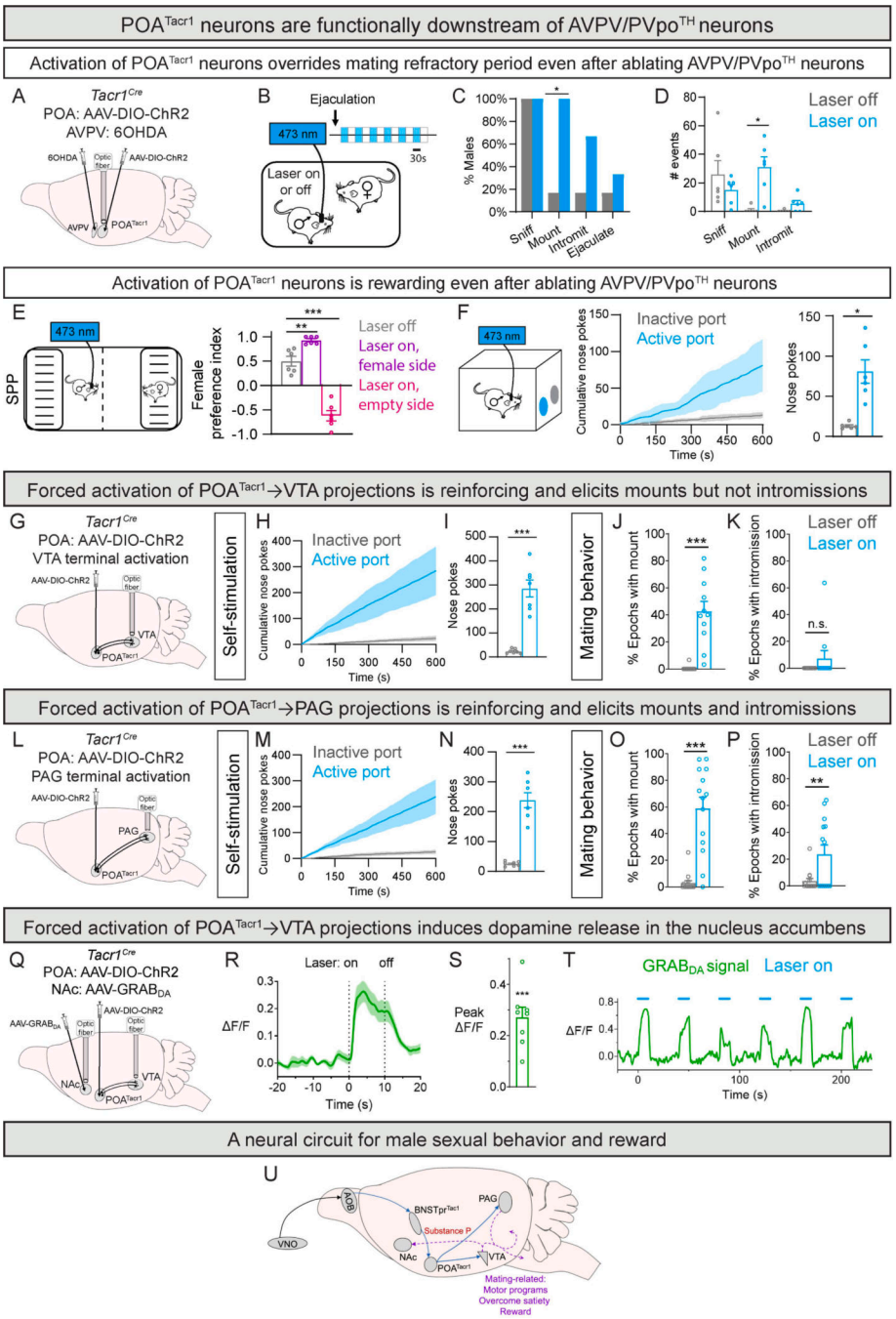

Figure 7: The BNSTpr^{Tac1}→POA^{Tacr1} pathway is embedded in a neural circuit linking pheromone sensing to motor output and reward.

A-D. Strategy to activate POA^{Tacr1} neurons following bilateral ablation of AVPV/PVpoTH neurons with 6OHDA (10 μg in 1 μL) (A). Schematic of optogenetic activation of POA^{Tacr1} neurons in post-ejaculatory males interacting with females (B). Activation (30/30 s on/off) re-ignites mating drive, increasing the probability (C) and number (D) of mating routines.

E. Schematic of optogenetic activation of POA^{Tacr1} neurons in males lacking AVPV/$PVpo^{TH}$ neurons in the SPP test (left). Activation governs behavioral preference of males (right).

F. Schematic of optogenetic self-stimulation (0.5 s, 40 Hz) of POA^{Tacr1} neurons in males lacking AVPV/$PVpo^{TH}$ neurons (left). Males show more nose pokes to the active port (right).

G-K. Strategy for optogenetic activation of VTA termini of male POA^{Tacr1} neurons (G). Males show more nose pokes to the active port (H,I).

More mounts (J) but not intromissions (K) in light epochs in encounters with females.

L-P. Strategy for ptogenetic activation of PAG termini of POA^{Tacr1} neurons (L). Males show more nose pokes to the active port (M,N).

More mounts (O) and intromissions (P) in light epochs in encounters with females.

Q-T. Optogenetic activation of $POA^{Tacr1}\rightarrow$VTA projections induces DA release in NAc. Strategy for fiber photometry imaging of DA release in NAc during activation (Q).

PETP (R) and change in fluorescence (S) of NAc neurons during activation.

$GRAB_{DA}$ signal trace (T) during light epochs (laser 10 s on, 30 s off) shows time-locked DA release.

U. Schematic of the male mating circuit outlined in this study. $BNSTpr^{Tac1}$ neurons receive input from the AOB and release Substance P to potentiate activation of POA^{Tacr1} neurons. Activation of POA^{Tacr1} neurons is necessary and sufficient to elicit mating, and it re-motivates sexually satiated mice to mate and is rewarding. Projections of these cells to the VTA or PAG also drive mating, mating in satiated males, and reinforcement, and activation of VTA projections elicits DA release in NAc. Arrows indicate pathways established by prior work[79] (black) or from our study (blue). Dashed arrows (purple) indicate pathways emanating from VTA and PAG that remain to be identified and connect with centers that drive mating-related motor programs, establish a motivational state for sexual behavior, and make sexual behavior rewarding.

Mean ± SEM. n = 6 mice (A-F), n = 7 mice (H-I), n = 11 mice (J-K), n = 7 mice (M-N), n = 14 mice (O-P), n = 8 mice (Q-T). * $p < 0.05$, ** $p < 0.01$, *** $p < 0.001$.

See also Fig. S8,9; Tables S1,3; Data S1.

KEY RESOURCES TABLE

REAGENT or RESOURCE	SOURCE	IDENTIFIER
Antibodies		
Sheep anti-GFP	Biorad	Cat # 4745–1051; RRID: AB_619712
Rat anti-RFP	Chromotek	Cat # 5f8–100; RRID: AB_2336064
Rat anti-mCherry	ThermoFisher	Cat # M11217; RRID: AB_2536611
Rabbit anti-Fos	Synaptic Systems	Cat # 226 008; RRID: AB_2891278
Rabbit anti-Esr1	Millipore	Cat # 06–935; RRID: AB_310305
Rabbit anti-TH	Aves	Cat # TYH; RRID: AB_10013440
Donkey anti-sheep, Alexa 488 conjugate	Jackson ImmunoResearch	Cat # 713–545-147; RRID: AB_2340745
Donkey anti-rabbit, Alexa 488 conjugate	Jackson ImmunoResearch	Cat # 711–545-152; RRID: AB_2313584
Donkey anti-rat, Cy3 conjugate	Jackson ImmunoResearch	Cat # 712–165-150; RRID: AB_2340666
Donkey anti-rabbit, Cy3 conjugate	Jackson ImmunoResearch	Cat # 711–165-152; RRID: AB_2307443
Donkey anti-chicken, Cy5 conjugate	Jackson ImmunoResearch	Cat # 703–175-155; RRID: AB_2340365
Donkey anti-rabbit, Alexa 647 conjugate	Jackson ImmunoResearch	Cat # 711–605-152; RRID: AB_2492288
Bacterial and virus strains		
Recombinant adeno-associated virus: AAV1-Syn-DIO-GCaMP6s	Addgene	Addgene number: 100845
Recombinant adeno-associated virus: AAV9-EF1α-DIO-PPO:Venus	Addgene	Addgene number: 139505
Recombinant adeno-associated virus: AAV1-EF1α-DIO-hChR2(H134R):EYFP	Addgene	Addgene number: 20298
Recombinant adeno-associated virus: AAV1-hSyn-hChR2(H134R):EYFP	Addgene	Addgene number: 26973
Recombinant adeno-associated virus: AAV1-CAG-DIO-EGFP	Addgene	Addgene number: 59331
Recombinant adeno-associated virus: AAV1-CAG-DIO-tdTomato	Addgene	Addgene number: 28306
Recombinant adeno-associated virus: AAV9-hSyn-GRAB_DA2m	Addgene	Addgene number: 140553
Recombinant adeno-associated virus: AAV2-EF1α-DIO-hChR2(H134R):mCherry	UNC Vector Core	Addgene number: 20297
Recombinant adeno-associated virus: AAV2-EF1α-DIO-eNpHR3.0:mCherry	UNC Vector Core	Addgene number: 26966
Recombinant adeno-associated virus: AAV2-EF1α-DIO-mCherry	UNC Vector Core	Addgene number: 50462
Recombinant adeno-associated virus: AAVDJ-EF1α-DIO-hM4DGi:mCherry	UNC Vector Core	Addgene number: 50461
Recombinant adeno-associated virus: AAVDJ-EF1α-fDIO-hM4DGi:mCherry	UNC Vector Core	Cat # AV7932
Recombinant adeno-associated virus: AAVDJ-EF1α-fDIO-hChR2(H134R):EYFP	UNC Vector Core	Addgene number: 55639
Recombinant adeno-associated virus: AAVDJ-hSyn-DIO-mGFP-2A-Synaptophysin:mRuby	Virovek	Addgene number: 71760
Recombinant adeno-associated virus: AAV8.2-TRE-DIO-TVA:mCherry-2A-oG	Virovek	Addgene number: 166602

REAGENT or RESOURCE	SOURCE	IDENTIFIER
EnvA G-deleted Rabies-EGFP	Salk Institute	Lot # 02282016
Cholera Toxin Subunit B, Alexa Fluor 555	ThermoFisher Scientific	Cat # C34776
Cholera Toxin Subunit B, Alexa Fluor 647	ThermoFisher Scientific	Cat # C34778
Chemicals, Peptides, and Recombinant Proteins		
DAPI	Sigma-Aldrich	Cat # D9542; CAS # 28718-90-3
Clozapine-N-oxide (CNO)	Enzo Life Sciences	Cat # BML-NS105-0005
Estradiol	Sigma-Aldrich	Cat # E8875; CAS # 50-28-2
Progesterone	Sigma-Aldrich	Cat # P0130; CAS # 57-83-0
Substance P	Sigma-Aldrich	Cat # S6883; CAS # 137348-11-9
L-703,606	Sigma-Aldrich	Cat # L119; CAS # 351351-06-9
Picrotoxin	Sigma-Aldrich	Cat # P1675; CAS # 124-87-8
6OHDA	Sigma-Aldrich	Cat # H4381; CAS # 28094-15-7
Tetrodotoxin	Tocris	Cat # 1069; CAS # 18660-81-6
Experimental models: Organisms/Strains		
Mouse: *C57BL/6J*	The Jackson Laboratory	Stock # 000664; RRID: IMSR_JAX:000664
Mouse: *BALB/c*	Charles River	Stock # 028
Mouse: *Tac1*^{Cre}	The Jackson Laboratory	Stock # 021877; RRID: IMSR_JAX:021877
Mouse: *Tacr1*^{Cre}	Diagle et al., 2018	N/A
Mouse: *Tac1 null*	The Jackson Laboratory	Stock # 004103; RRID: IMSR_JAX:004103
Mouse: *Esr1*^{Flpo}	The Jackson Laboratory	Stock # 037009; RRID: IMSR_JAX:037009
Software and Algorithms		
ImageJ	NIH	https://imagej.nih.gov/ij/index.html; RRID: SCR_003070
MATLAB	MathWorks	https://www.mathworks.com/products.html; RRID: SCR_001622
GraphPad Prism 6	GraphPad Software	https://www.graphpad.com/scientificsoftware/prism/; RRID: SCR_002798
Inscopix Data Processing Software	Inscopix Inc.	https://www.inscopix.com/software-analysisminiscope-imaging#software_idps